

# The global monsoon system representation in BAM-v1.2 and HadGEM3 climate simulations

Iracema F. A. Cavalcanti<sup>1</sup>  | Dayana C. Souza<sup>1</sup> | Paulo Y. Kubota<sup>1</sup> |  
Caio A. S. Coelho<sup>1</sup>  | Silvio N. Figueroa<sup>1</sup> | Jessica C. A. Baker<sup>2</sup>

<sup>1</sup>Centro de Previsão de Tempo e Estudos Climáticos, Instituto Nacional de Pesquisas Espaciais (CPTEC/INPE), São José dos Campos, Brazil

<sup>2</sup>School of Earth and Environment, Institute for Climate and Atmospheric Science, University of Leeds, Leeds, UK

## Correspondence

Iracema F. A. Cavalcanti, Centro de Previsão de Tempo e Estudos Climáticos, Instituto Nacional de Pesquisas Espaciais (CPTEC/INPE), Av. dos Astronautas, 1758 São José dos Campos, SP, Brazil.  
Email: [iracema.cavalcanti@inpe.br](mailto:iracema.cavalcanti@inpe.br)

## Funding information

Conselho Nacional de Desenvolvimento Científico e Tecnológico, Grant/Award Number: 306393/2018-2; CAPES, Grant/Award Number: 88887.469114/2019-00; CNPq, Grant/Award Number: 305206/2019-2; Coordenação de Aperfeiçoamento de Pessoal de Nível Superior (CAPES), Grant/Award Number: 88887145932/2017-01; Fundação de Amparo à Pesquisa do Estado de São Paulo (FAPESP)-Belmont Forum, Grant/Award Number: CLIMAX-2015/50687-8

## Abstract

The features of monsoon systems in the Northern and Southern Hemispheres are analysed in climate simulations of two atmospheric models: the Brazilian Global Atmospheric Model version 1.2 (BAM-v1.2) and the UK Met Office Hadley Centre Global Environment Model version 3 (HadGEM3). The results are compared to GPCP precipitation and ERA5 datasets. Although they have different configurations and parameterizations, the purpose is to evaluate their ability in representing key features of the global monsoon system. The spatial extent of the monsoon domains is well simulated by the models, as well as the main characteristics of the monsoons, although precipitation biases are noticed in the regions affected by the systems, consistent with vertical motion and moisture flux biases. The largest precipitation biases are found in the West Pacific Monsoon Region, extended to the east, and in the Australia Monsoon Region extended to the Maritime continent. Deficiencies in precipitation can be related to inaccuracy of vertical motion and humidity flux, as well as to the lack of air–sea interaction. However, the atmospheric circulation features at low and high levels are well represented in all monsoon regions, as well as the annual cycle of precipitation in those regions by both models. The divergence at high levels and convergence at low levels associated with ascending air movement and precipitation in monsoon regions are well represented by the models. An analysis of two monsoon indices at eight monsoon regions showed the models are generally able to simulate the relationship between precipitation and circulation features. In the majority of years, the signs of indices from the models agree with observations. Correlations of precipitation and circulation indices between models and observations show statistically significant values for some monsoon regions. The results obtained contribute to improving knowledge about global monsoon features and their representation in the two models.

## KEYWORDS

atmospheric circulation, BAM-v1.2, climate simulation, global monsoon, HadGEM3, monsoon indices, precipitation

This is an open access article under the terms of the [Creative Commons Attribution-NonCommercial-NoDerivs](https://creativecommons.org/licenses/by-nc-nd/4.0/) License, which permits use and distribution in any medium, provided the original work is properly cited, the use is non-commercial and no modifications or adaptations are made.

© 2022 The Authors. *International Journal of Climatology* published by John Wiley & Sons Ltd on behalf of Royal Meteorological Society.

## 1 | INTRODUCTION

Monsoon regions present a defined precipitation cycle and associated circulation features, which characterize aspects of the climate in several continents. The precipitation variability in these regions can affect many socio-economic sectors, including agriculture and worldwide water resources. The concept of global monsoon was discussed by Wang and Ding (2008) and Wang *et al.* (2011) as the representation of the two main modes of precipitation and low-level winds variability: a solstitial mode and an equinoctial mode. The solstitial mode is identified in the first empirical orthogonal function (EOF) pattern of precipitation and it is similar to the global precipitation domain configuration obtained by the precipitation annual range (MJJAS minus NDJFM) in the Northern Hemisphere (NH) and (NDJFM minus MJJAS) in the Southern Hemisphere (SH). The equinoctial mode is obtained in the second EOF of precipitation and the pattern is similar to the precipitation difference between April–May and October–November. Trenberth *et al.* (2000) discussed the global monsoon through the mean annual cycle of the large-scale overturning in the divergent atmospheric circulation. He analyses the atmospheric cells as part of the overturning.

The global monsoon domain comprises regions where the precipitation annual range exceeds 300 mm (Wang and Ding, 2008) or  $2.5 \text{ mm day}^{-1}$  (Wang *et al.*, 2011) and the Monsoon Precipitation Index (MPI), calculated by the annual range normalized by the annual mean precipitation, exceeds 0.5. These regions characterize the highest precipitation in each summer hemisphere and show a reversal pattern in the winter hemisphere. Using the monsoon domain definition, Yim *et al.* (2014) identified eight monsoons in the global system: Indian, Western North Pacific, East Asian, North American, South American, Australian, Northern African and Southern African. Although they have regional features, the seasonal precipitation and circulation cycles present similar characteristics.

Climate predictions and projections using dynamic models are important tools for management strategies and planning actions to cope with precipitation variability and changes. The ability of dynamic models in representing the global monsoon has been presented in several studies such as Kim *et al.* (2008), analysing Coupled Model Intercomparison Project (CMIP)-Phase 3 (CMIP3) models, Kitoh *et al.* (2013) and Hsu *et al.* (2013), using CMIP-Phase 5 (CMIP5) models and Wang *et al.* (2020), evaluating CMIP-Phase 6 (CMIP6) models. The main global monsoon climatological features are represented in these models and although the performance has improved in CMIP6, there are still precipitation

biases in several regions around the world (Wang *et al.*, 2020). A CMIP6 model intercomparison for global monsoons is presented in Zhou *et al.* (2016), where several experiments are described, including orographic perturbations and sea surface temperature changes in the Pacific and Atlantic Oceans, among others. The purpose was to improve the understanding of processes that affect the global monsoon variability. Global monsoon changes in CMIP6 projections were discussed in several studies, such as Zhang *et al.* (2018a, 2018b), Zhang *et al.* (2019), Chen *et al.* (2020), Zhou *et al.* (2020a) and Zhou *et al.* (2020b).

The representation of regional monsoons in climate models has also been investigated in several studies, as the Indian Monsoon (Jain *et al.*, 2018; Kumar and Sarthi, 2021), Asian Monsoon (Boo *et al.*, 2011; Song and Zhou, 2014a; 2014b; Xin *et al.*, 2020), Asia-Australia Monsoon (Zhou *et al.*, 2009a), North American Monsoon (Pascale *et al.*, 2016; García-Franco *et al.*, 2020), South American Monsoon (Carvalho and Cavalcanti, 2016; Cavalcanti and Raia, 2017; Coelho *et al.*, 2021a), Australia Monsoon (Colman *et al.*, 2011; Huang *et al.*, 2019) and African Monsoon (Hannak *et al.*, 2017; Raj *et al.*, 2019). While regional monsoons studies assess the ability of models to represent regional monsoon features, global monsoon analyses focus on the representation of large-scale features from a global perspective. There is therefore a need to further assess global monsoon features in global climate models to advance knowledge of the ability of these models to simulate this important climatic feature, and to build confidence for the use of these models for climate predictions and projections for the future.

The objective of this paper is to evaluate the main features of the global monsoon system in two atmospheric models, the Brazilian Global Atmospheric Model (BAM-v1.2) and the atmospheric component of the UK Met Office Hadley Centre Global Environment Model version 3 (HadGEM3). This is the first comparative assessment of these two models in representing global monsoon features, providing a detailed analysis of eight specific monsoon regions all around the world. The common typical features of atmospheric circulation, precipitation and other variables in eight monsoon regions are discussed. Particular attention is devoted to performing a quantitative assessment of monsoon features by comparing model-simulated and observed patterns, as well as temporal association between precipitation and circulation monsoon indices. The knowledge of these two models behaviour in monsoon regions is important to further use in climate predictions and projections.

Datasets and methods are shown in section 2, and the global monsoon features are discussed in section 3. The

annual cycle and indices of the regional monsoons are presented in section 4, and discussion as well as conclusion are disclosed in section 5.

## 2 | DATASETS AND METHODS

### 2.1 | Datasets

For the observational datasets, the precipitation is from the Global Precipitation Climatology Project (GPCP), (Adler *et al.*, 2003), horizontal wind (u and v), vertical wind (omega), specific humidity and precipitable water from European Centre for Medium-Range Weather Forecasts Reanalysis (ERA-5) (Hersbach *et al.*, 2020) and Outgoing Longwave Radiation (OLR) provided by NOAA (Liebmann and Smith, 1996) for the period of 1981 to 2010.

Climatological simulations of the period 1981–2010 obtained from two atmospheric models were used to analyse the global monsoon. One is the Brazilian Atmospheric Model (BAM-v1.2), which is the current weather and seasonal climatic prediction operational CPTEC global model (Coelho *et al.*, 2021b) and it is the atmospheric component of the Brazilian Earth System Model (BESM) used for climate integrations (Veiga *et al.*, 2019).

As described in Figueroa *et al.* (2016), the BAM dynamical core is a hydrostatic semi-implicit spectral model designed with two options, one for weather forecasting with the semi-Lagrangian scheme and other for climate integration with the Eulerian transport scheme. The last option is used in this study, except for the moisture and microphysical variables, when a monotonic two-time-level semi-Lagrangian scheme is used. The BAM-1.2 physical processes components used for performing the climate simulation are the same as described in Coelho *et al.* (2021b) and presented in Table 1. The climate simulation was performed with resolution of T126L42, which corresponds to a horizontal resolution of ~100 km and 42 vertical levels.

The other model is the atmospheric component of the UK Met Office Hadley Centre Global Environment Model version 3 (HadGEM3; Ridley *et al.*, 2018; Williams *et al.*, 2018), with ~60 km horizontal resolution and 85 vertical levels. This model was used by Zhang *et al.* (2018a, 2018b), who showed improvements of precipitation and atmospheric circulation in global monsoon simulations with increased resolution. Both simulations were produced using observed Sea Surface Temperature (SST) and sea ice prescribed as boundary conditions.

For BAM-1.2 simulations, carbon dioxide (CO<sub>2</sub>) concentration was kept constant at 370 ppm during the

**TABLE 1** Physical processes components of BAM-v1.2

Deep convection	Revised simplified Arakawa-Shubert deep convection scheme (Han and Pan, 2011), with the following adjustments: 1 – momentum calculation including pressure gradient generated by convective cells, 2 – entrainment parameters calibration
Shallow convection	Tiedtke (1989)
Microphysics	Morrison <i>et al.</i> (2005, 2009)
Land surface	IBIS/CPTEC (Kubota, 2012)
Longwave radiation scheme	CLIRAD-LW (Chou <i>et al.</i> , 2001)
Shortwave radiation scheme	CLIRAD-SW (Chou and Suarez, 1999) modified by Tarasova and Fomin (2000)
Planetary boundary layer	Moist diffusion scheme (Bretherton and Park, 2009) and the following adjustments: 1 – interactive calculation between stratiform cloudiness and the vertical diffusion coefficient, and 2 – improved saturation vapour pressure calculation (Souza <i>et al.</i> , 2019)
Thermal plume for convective boundary layer	Rio and Houdin (2008)
Aerosol optical depth	Yu <i>et al.</i> (2006)
Cloud fraction	Scheme based on Slingo (1987). The scheme generates four types of clouds: convective, high, middle and low clouds. In this scheme, the influence of the cloud fraction calculation based on probability distribution function (PDF) generalized log-normal distribution, was incorporated
Optical properties	Ice optical properties for shortwave (Ebert and Curry, 1992) Liquid optical properties for shortwave (Slingo's data for cloud particle radiative properties; Slingo, 1989) Liquid optical properties for longwave (Slingo's data for cloud particle radiative properties; Slingo, 1984) Ice optical properties for longwave (Ebert and Curry, 1992) modified by Andrew Conley

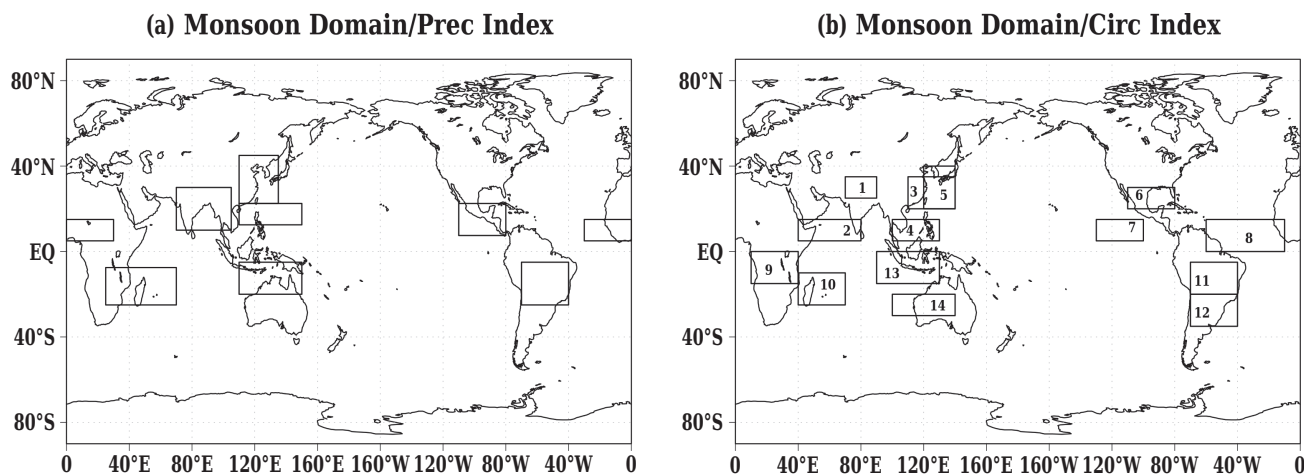


**FIGURE 1** Monsoon domains for (a) areal precipitation and precipitation index (PI), (b) circulation index (CI). Numbers in (b) refer to areas taken to calculate the circulation index

integration. Except for this concentration, the simulations follow the protocol of the Atmospheric Global Models Intercomparison Project (AMIP), where the only forcing is the observed SST (in AMIP the  $\text{CO}_2$  concentration varies annually, as stated in Coelho *et al.*, 2021b). The same variables of observations are analysed using the ensemble of four (five) BAM-v1.2 (HadGEM3) members. These two models were used to analyse land-atmosphere interactions over South America (Baker *et al.*, 2021), showing results consistent with several CMIP6 models, and also to assess the South America Monsoon System representation (Coelho *et al.*, 2021a).

## 2.2 | Methods

The spatial extent of the global monsoon domain was analysed following Wang *et al.* (2011), who used  $2.5 \text{ mm}\cdot\text{day}^{-1}$  as the threshold for the summer-winter precipitation difference (annual range) to define the monsoon regions. Normalizing the annual range by the annual mean precipitation (i.e., dividing the annual range by the annual mean precipitation), the monsoon precipitation intensity (MPI) is calculated in each grid point. The intensity can also be obtained using two monsoon indices established by Yim *et al.* (2014): a precipitation index (PI) and a circulation index (CI). The nomenclature used in Yim *et al.* (2014) as Summer Monsoon in the eight regions is changed to Monsoon System; for example, Indian Summer Monsoon (ISM) is called Indian Monsoon System (IMS) here. The other monsoon systems are East Asian Monsoon System (EAMS), Western North Pacific Monsoon System (WNPMS), North America Monsoon System (NAMS), Northern African Monsoon System (NAFMS), Southern African Monsoon

**TABLE 2** Areas that were taken to calculate the precipitation index and the annual cycle of precipitation for each monsoon region

Regional monsoon Precipitation domain	Areas
IMS	$10^\circ\text{--}30^\circ\text{N}$ , $70^\circ\text{--}105^\circ\text{E}$
WNPMS	$12.5^\circ\text{--}22.5^\circ\text{N}$ , $110^\circ\text{--}150^\circ\text{E}$
EAMS	$22.5^\circ\text{--}45^\circ\text{N}$ , $110^\circ\text{--}135^\circ\text{E}$
NAMS	$7.5^\circ\text{--}22.5^\circ\text{N}$ , $110^\circ\text{--}80^\circ\text{W}$
NAFMS	$5^\circ\text{--}15^\circ\text{N}$ , $30^\circ\text{W--}30^\circ\text{E}$
SAFMS	$7.5^\circ\text{--}25^\circ\text{S}$ , $25^\circ\text{--}70^\circ\text{E}$
SAMS	$5^\circ\text{--}25^\circ\text{S}$ , $70^\circ\text{--}40^\circ\text{W}$
AUSMS	$5^\circ\text{--}20^\circ\text{S}$ , $110^\circ\text{--}150^\circ\text{E}$

**TABLE 3** Areas that were taken to calculate the circulation index for each monsoon region indicated in Figure 1b

Region	Definition of the circulation index
IMS	U2 ( $5^\circ\text{--}15^\circ\text{N}$ , $40^\circ\text{--}80^\circ\text{E}$ ) minus U1 ( $25^\circ\text{--}35^\circ\text{N}$ , $70^\circ\text{--}90^\circ\text{E}$ )
WNPMS	U4 ( $5^\circ\text{--}15^\circ\text{N}$ , $100^\circ\text{--}130^\circ\text{E}$ ) minus U3 ( $20^\circ\text{--}35^\circ\text{N}$ , $110^\circ\text{--}140^\circ\text{E}$ )
EAMS	V5 ( $20^\circ\text{--}40^\circ\text{N}$ , $120^\circ\text{--}140^\circ\text{E}$ )
NAMS	U7 ( $5^\circ\text{--}15^\circ\text{N}$ , $130^\circ\text{--}100^\circ\text{W}$ ) minus U6 ( $20^\circ\text{--}30^\circ\text{N}$ , $110^\circ\text{--}80^\circ\text{W}$ )
NAFMS	U8 ( $0^\circ\text{--}15^\circ\text{N}$ , $60^\circ\text{--}10^\circ\text{W}$ )
SAFMS	U9 ( $15^\circ\text{S--}0^\circ$ , $10^\circ\text{--}40^\circ\text{E}$ ) minus U10 ( $25^\circ\text{--}10^\circ\text{S}$ , $40^\circ\text{--}70^\circ\text{E}$ )
SAMS	U11 ( $20^\circ\text{--}5^\circ\text{S}$ , $70^\circ\text{--}40^\circ\text{W}$ ) minus U12 ( $35^\circ\text{--}20^\circ\text{S}$ , $70^\circ\text{--}40^\circ\text{W}$ )
AUSMS	U13 ( $15^\circ\text{S--}0^\circ$ , $90^\circ\text{--}130^\circ\text{E}$ ) minus U14 ( $30^\circ\text{--}20^\circ\text{S}$ , $100^\circ\text{--}140^\circ\text{E}$ )

Note: U and V are wind anomaly components at 850 hPa.

System (SAFMS), Australian Monsoon System (AUMS) and South American Monsoon System (SAMS). The North Hemisphere monsoons are analysed in the boreal summer: June, July, August (JJA) and the South Hemisphere monsoons, in the austral summer: December, January, February (DJF).

The monthly PI is obtained by calculating areal average precipitation anomalies over each monsoon region, shown in Figure 1a and Table 2, divided by the standard deviation of the area-average precipitation time series (1981–2010). The monthly circulation index, related to circulation that affects each monsoon, in Figure 1b and Table 3, is calculated using the meridional shear of zonal wind anomaly at 850 hPa for WNPMS, IMS, NAMS in the Northern Hemisphere; and SAMS, SAFMS, AUSMS, in the Southern Hemisphere. In EAMS, the index is obtained from the meridional wind anomaly at 850 hPa,

and in NAFMS, from the zonal wind anomaly at 850 hPa. The zonal and meridional winds anomalies are normalized also by the standard deviation, before doing the areal mean in each monsoon region. The precipitation and circulation indices are well correlated and represent the strength of the monsoon. They can be used for monitoring, predictions and studies of variability and predictability of regional monsoons (Yim *et al.*, 2014). Therefore, these monthly indices and their correlations were calculated for the eight monsoon regions.

In order to verify the regions where the models overestimate or underestimate precipitation, vertical motion and humidity flux divergence, biases of these variables were calculated through differences between model simulations and observational climatology (GPCP and ERA5). To assess the correspondence in terms of association between models simulated and observed spatial

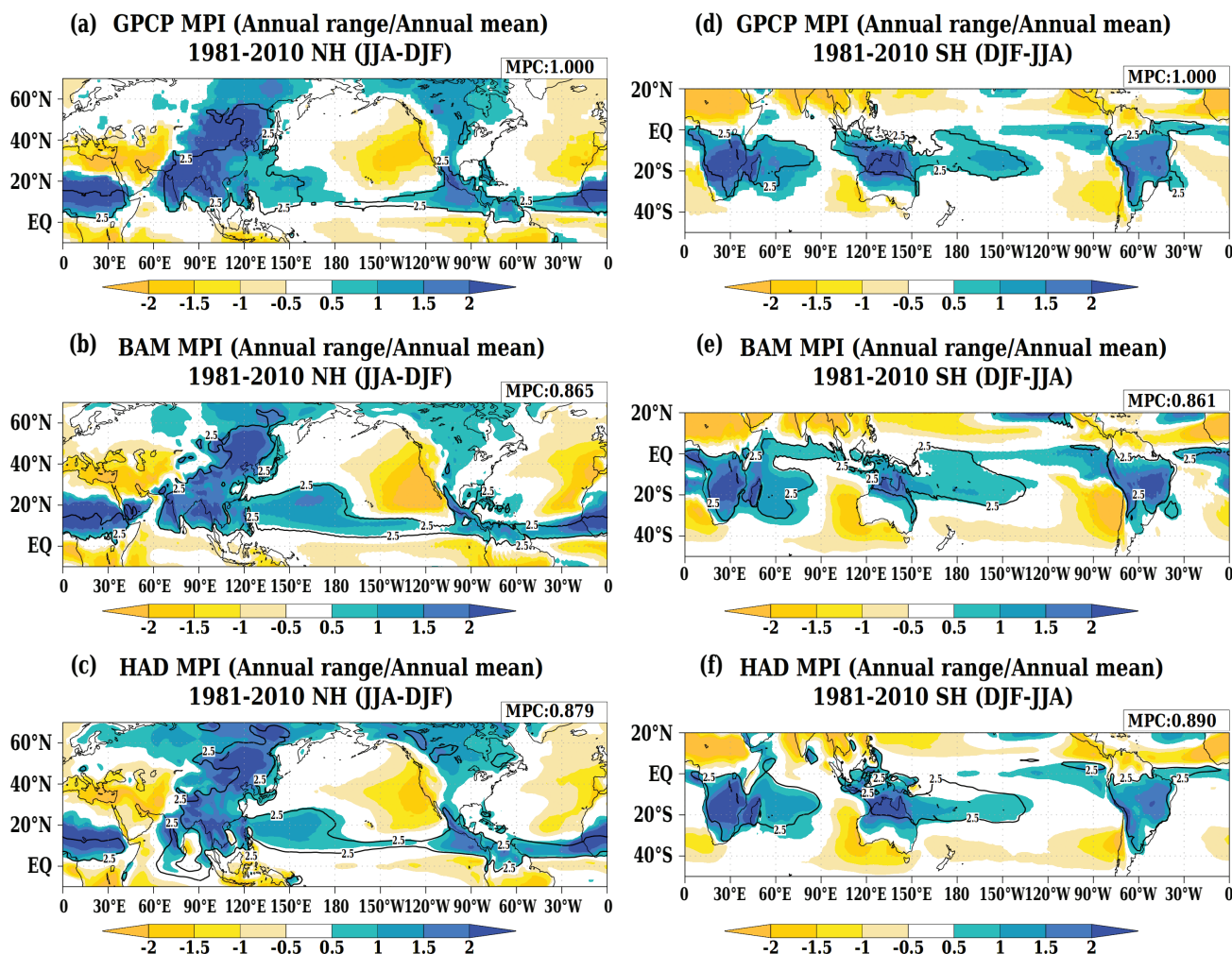


**FIGURE 2** Monsoon precipitation intensity (MPI): colour and precipitation  $\geq 2.5 \text{ mm-day}^{-1}$ : contour. Observed (top), BAM-v1.2 (middle), HadGEM3 (bottom). left panel: NH (JJA-DJF), right panel: SH (DJF-JJA). The numbers at the upper right corners of each panel are the MPI pattern correlation (MPC) values computed between the models and observed (GPCP) MPI values shown in these figure panels [Colour figure can be viewed at [wileyonlinelibrary.com](http://wileyonlinelibrary.com)]

patterns, pattern correlation values between climatological mean patterns of models simulations and observations (GPCP or ERA5) were calculated. Additionally, correlations between observed precipitation (GPCP) and models simulated precipitation over the 1981–2010 period for JJA and DJF were calculated at each grid point.

### 3 | GLOBAL MONSOON FEATURES

The spatial extent of the global monsoons domain is presented in Figure 2 (contours), where the intensity is displayed (colours). Figure 2a indicates the observed Northern Hemisphere Monsoons, where we can see three

regions delimited by the threshold of  $2.5 \text{ mm} \cdot \text{day}^{-1}$ . The largest area comprises the IMS, EAMS and WNPMS and the former two present the highest MPI. It is seen that the NAMS comprises Central America, Mexico and the extreme north of South America, extending to the Pacific Ocean. NAFMS domain extends to the Atlantic Ocean, linked to the Intertropical Convergence Zone (ITCZ) seasonal variability. In the Southern Hemisphere (Figure 2d) there are also three monsoon regions, SAFMS, AUMS and SAMS. While in SAFMS and AUSMS, the domains extend to large areas of the Indian and Pacific Ocean, respectively, SAMS extends to a small area eastward over the South Atlantic Ocean and also to the Atlantic ITCZ region. These areas over the southern oceans indicate regions of the Convergence Zones: Indian Convergence

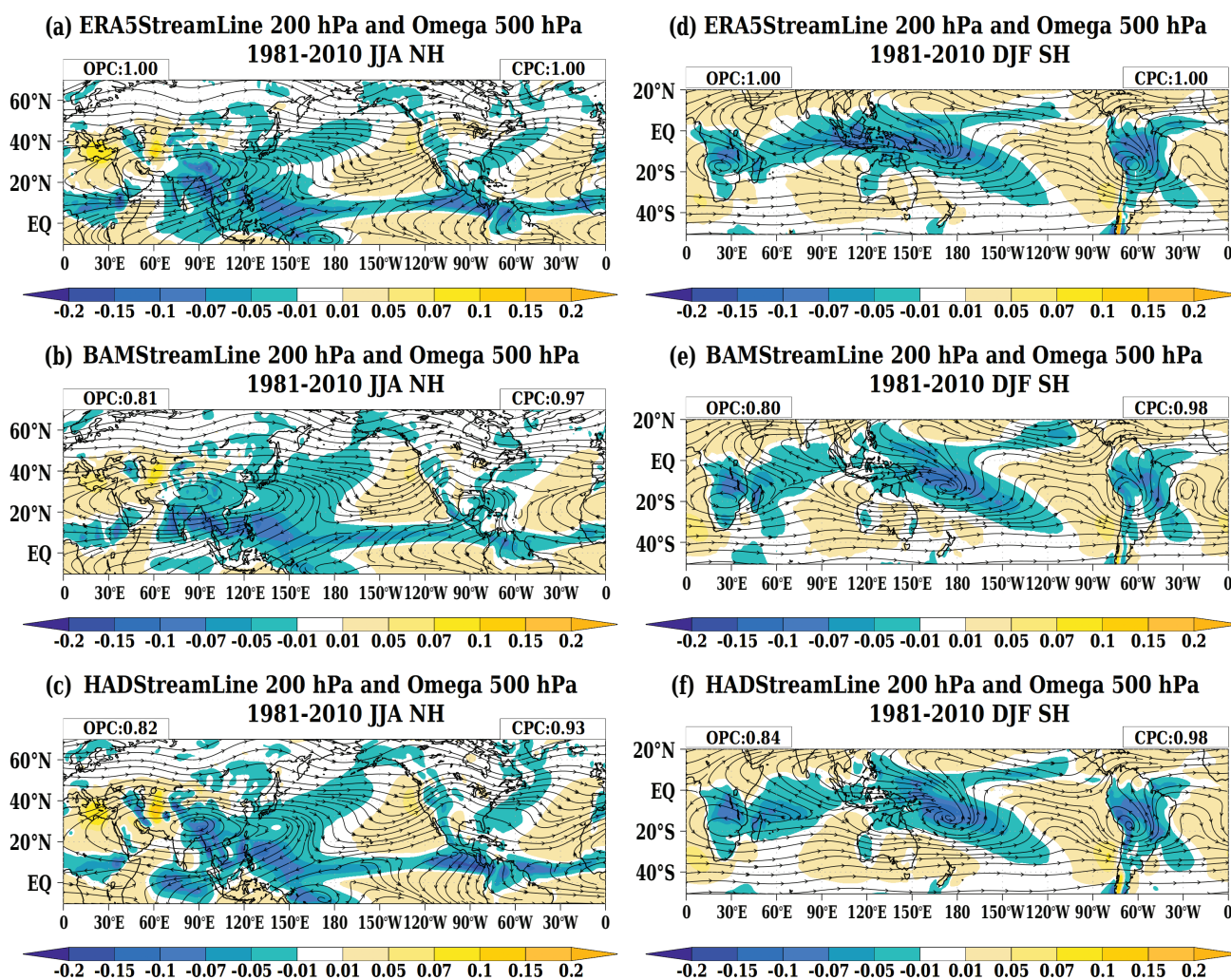


**FIGURE 3** Omega ( $\text{Pa} \cdot \text{s}^{-1}$ ) at 500 hPa and streamlines at 200 hPa. ERA5 (top), BAM-v1.2 (middle), HadGEM3 (bottom). Left panel: NH, right panel: SH. The numbers at the upper right corners of each panel are the circulation pattern correlation (CPC) values computed between the models and observed (ERA5) zonal and meridional wind components values used to produce these figure panels. The numbers at the upper left corners of each panel are the vertical velocity (omega) pattern correlation (OPC) values computed between the models and observed (ERA5) values shown in these figure panels [Colour figure can be viewed at [wileyonlinelibrary.com](http://wileyonlinelibrary.com)]

Zone (ICZ), South Pacific Convergence Zone (SPCZ) and South Atlantic Convergence Zone (SACZ). In the NH (SH) there are three relatively dry regions (drier in summer than winter) to the northwest (southwest) of the three monsoon domains at the subtropical latitudes. The strong ascending motion in the monsoon regions, which can be seen through negative values in the omega field of Figure 3, results in subsidence over these dry areas (seen by the positive values in the omega field of Figure 3).

Except in the Asia monsoon region, the continental spatial extent and intensities of monsoon precipitation are reasonably well captured by the BAM-v1.2 (Figure 2b,e) and HadGEM3 (Figure 2c,f) models, but the intensities over the Pacific Ocean are overestimated in the NH and underestimated in the SH. The intensity in

the relatively dry areas to the west of North America and North Africa are overestimated by BAM-v1.2, while HadGEM3 represents similar observed intensities. However, for the SH, HadGEM3 overestimates the dry areas to the southwest of South America and west of Australia, while BAM-v1.2 overestimates the intensities of all three dry areas to the southwest of the monsoon regions. This overestimation is related to the deficiency of interactions between radiation and clouds in those regions, which was detected in previous studies (Tarasova and Cavalcanti, 2002; Barbosa *et al.*, 2008; Cavalcanti *et al.*, 2020; Coelho *et al.*, 2021a; 2021b). In these areas, there is insufficient absorption of longwave radiation in the model atmosphere, which is related to the reduced optical depth in the clouds. These previous studies also

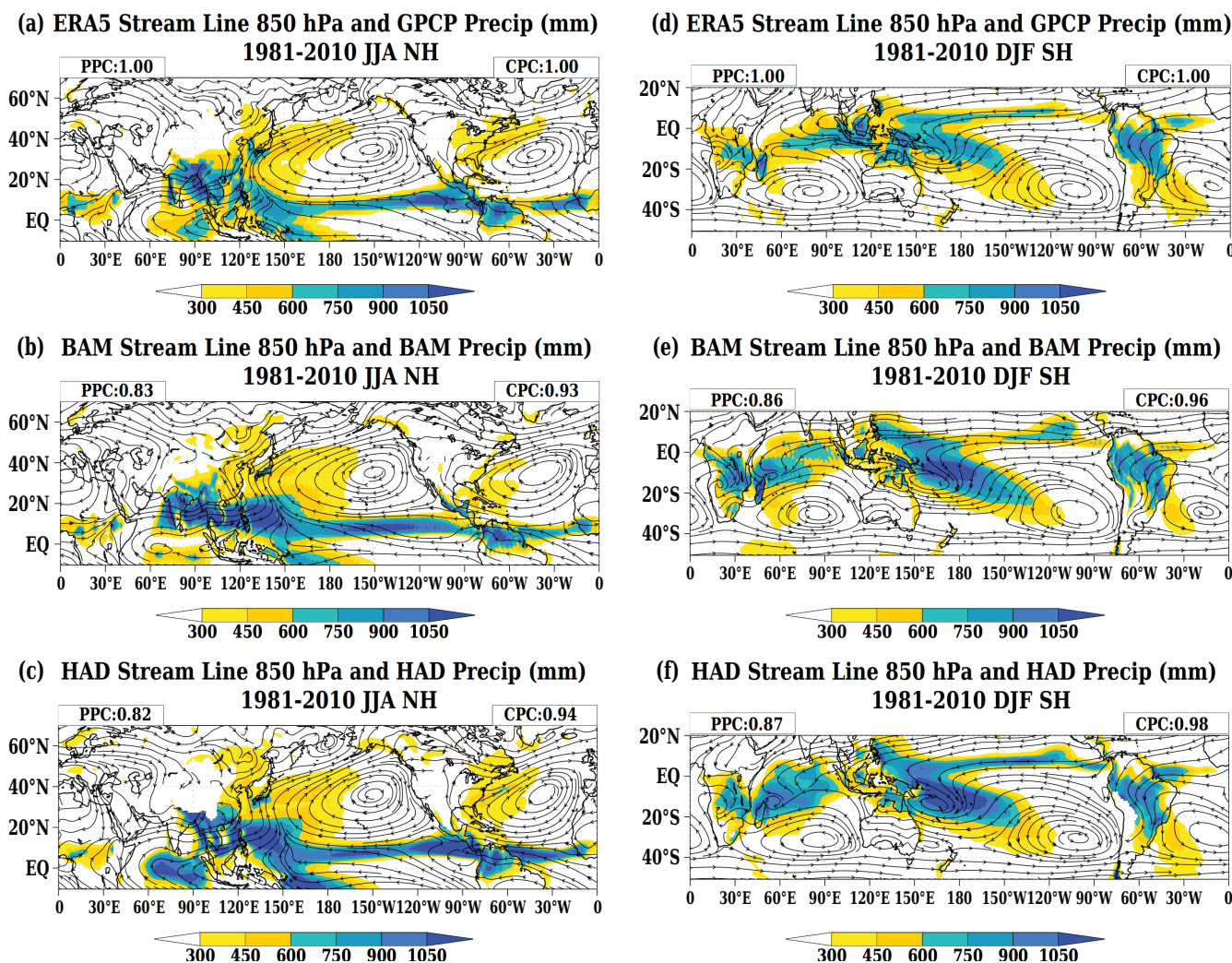


**FIGURE 4** Precipitation (mm) and wind field at 850 hPa. GPCP and ERA5 (top), BAM-v1.2 (middle), HadGEM3 (bottom). Left panel: NH, right panel: SH. The numbers at the upper right corners of each panel are the circulation pattern correlation (CPC) values computed between the models and ERA5 zonal and meridional wind components values shown in these figure panels. The numbers at the upper left corners of each panel are the precipitation pattern correlation (PPC) values computed between the models and observed (GPCP) values shown in these figure panels [Colour figure can be viewed at [wileyonlinelibrary.com](https://onlinelibrary.wiley.com)]

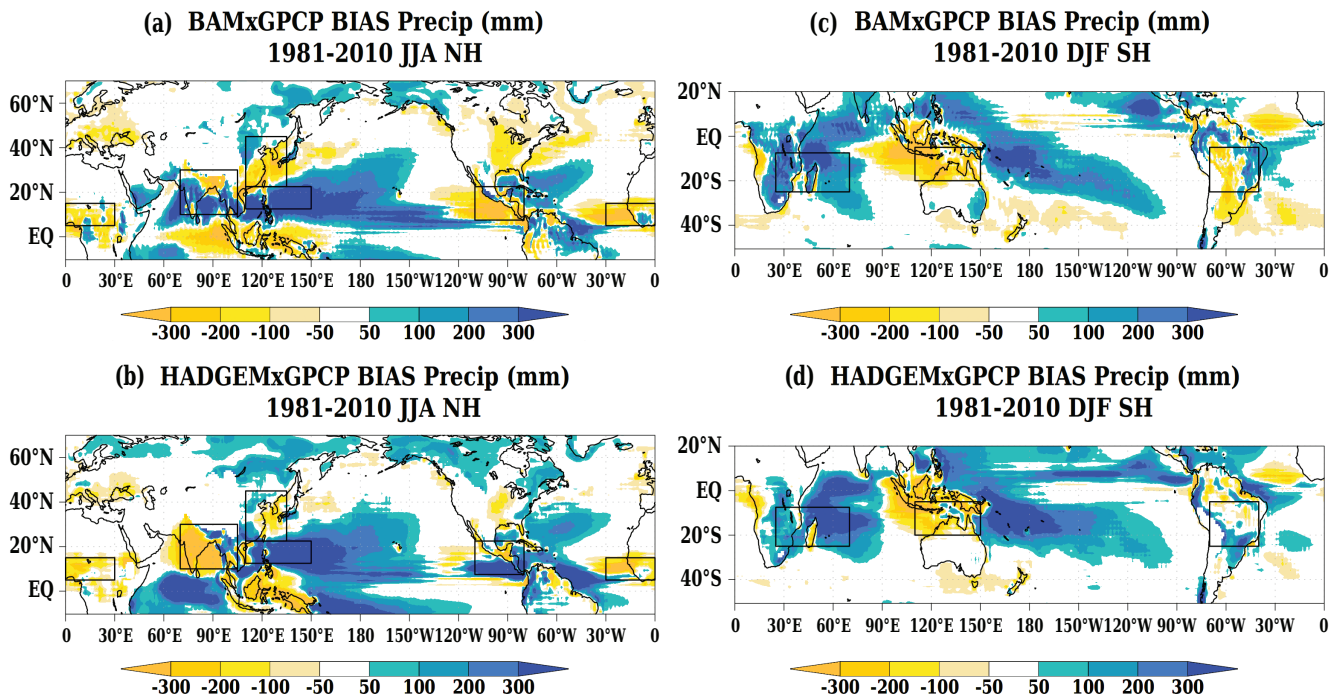


FIGURE 5 Precipitation bias (mm) calculated between models BAM-v1.2 (a, c), HadGEM3 (b, d) and GPCP. Left panel: NH, right panel: SH. Monsoon areas (black boxes) [Colour figure can be viewed at [wileyonlinelibrary.com](http://wileyonlinelibrary.com)]

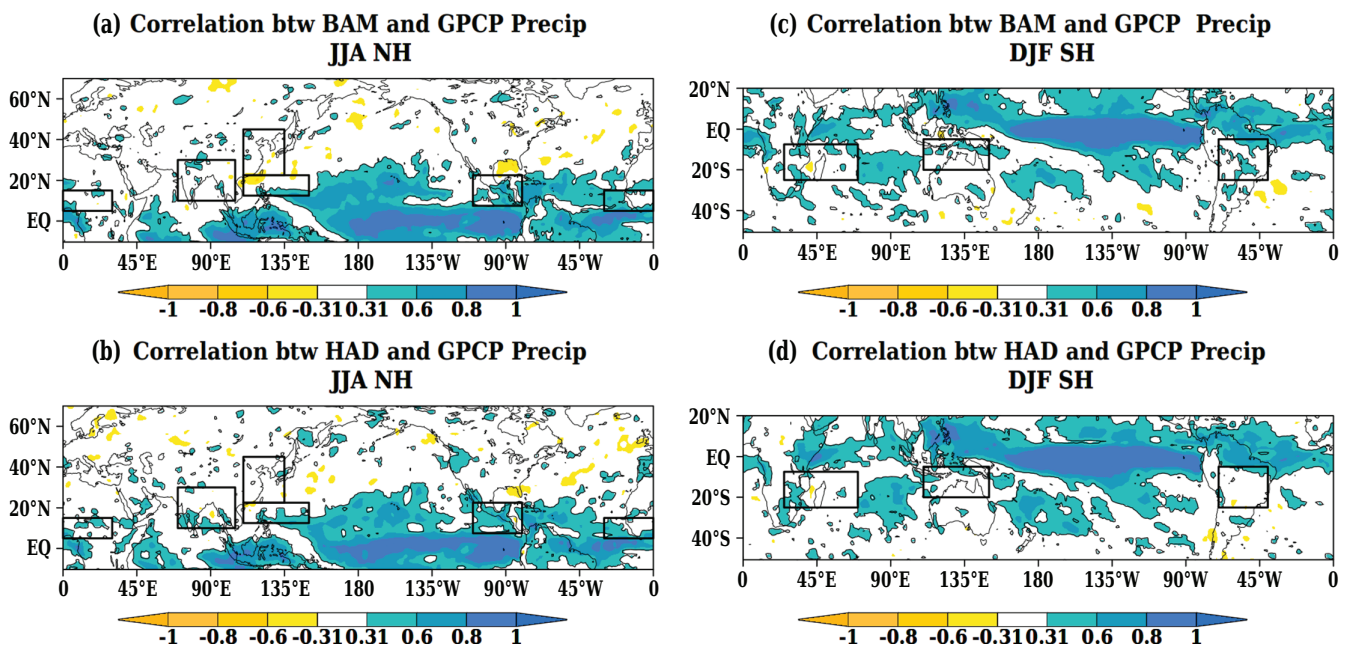


FIGURE 6 Correlation between observed precipitation (GPCP) and simulated precipitation by BAM-v1.2 and HadGEM3, over the 1981–2010 period for boreal summer (JJA, first column) and austral summer (DJF, second column). Left panel: NH, right panel: SH. Correlation values above 0.31 (black contour) are statistically significant using the  $t$  test for correlation at the 10% level [Colour figure can be viewed at [wileyonlinelibrary.com](http://wileyonlinelibrary.com)]

show an overestimation of shortwave radiation, due to reduced trace gases and aerosols as well as misrepresentation of clouds–atmosphere interactions. The MPI

pattern correlation values between the observed and model simulated patterns for BAM-v1.2 and HadGEM3 in the NH are 0.865 and 0.879, respectively, and in the

SH are 0.861 and 0.890, respectively, indicating good performance of both models in representing the global monsoon spatial structure.

The typical anticyclonic feature of monsoon at high levels are well reproduced by the models: the Tibetan High and the Mexican High in the NH (Figure 3a–c) and Bolivian High, African and West Pacific anticyclonic circulations in the SH (Figure 3d–f). The models also capture the mean trough at high levels to the east of the anticyclonic circulations, although the Mexican High is not reproduced by the HadGEM3 model (Figure 3c). This deficiency reduces the circulation pattern correlation at high levels in the NH between ERA5 and HadGEM3. While the circulation pattern correlation for BAM-v1.2 is 0.97, for HadGEM3 the circulation pattern correlation is 0.93. In the SH the circulation pattern correlation is 0.98 for both models.

Meanwhile, the ascent and subsident regions, identified with negative and positive omega values respectively in Figure 3, are well represented by the two models, although the omega pattern correlations between ERA5 and model simulations are lower than the circulation pattern correlations. For the NH, the omega pattern correlations are 0.81 (BAM-v1.2) and 0.82 (HadGEM3), while for the SH the omega pattern correlations are 0.80 (BAM-v1.2) and 0.84 (HadGEM3). These circulation features are common in the monsoon regions, which were discussed by Chen (2003) from a planetary perspective.

The models reproduce the mean characteristics of precipitation and low-level flow (Figure 4). In the NH,

the typical inland flow from Indian Ocean brings humidity to India and southeastern Asia, where large precipitation values are noticed (Figure 4a). BAM-v1.2 and HadGEM3 models simulate this typical pattern (Figure 4b,c), but overestimate rainfall over southeastern Asia and the maximum precipitation extends further eastward than in the observations. The northward flow from Indonesia and from the North Pacific Subtropical High (NPSH), which brings the humidity to increase precipitation in eastern Asia during the boreal summer season, are shifted eastward in the model simulations. As this subtropical high has an important role on the EAMS (Lu and Dong, 2001; Song and Zhou, 2014b), changes in its position can affect monsoon features. NPSH inter-annual variability is influenced by SST anomalies of the North and equatorial Pacific and by changes in the sensible heating over the Tibetan High, as discussed in Cherchi *et al.* (2018). Therefore, the model errors in the NPSH can be related to errors in these other variables. The typical pattern of more precipitation in the southern area of EAMS but less in the northern area (Figure 4a–c) is captured by the models. Nevertheless, BAM-v2.1 underestimates large areas of EAMS and HadGEM3 overestimates the precipitation in some areas of the western sector (Figure 5a,b). This typical pattern was also reproduced by CMIP5 and CMIP6 multimodels (Xin *et al.*, 2020). They attribute the precipitation bias to the topography in the region. Model biases in reproducing the monsoon rainfall over East Asia are partly due to

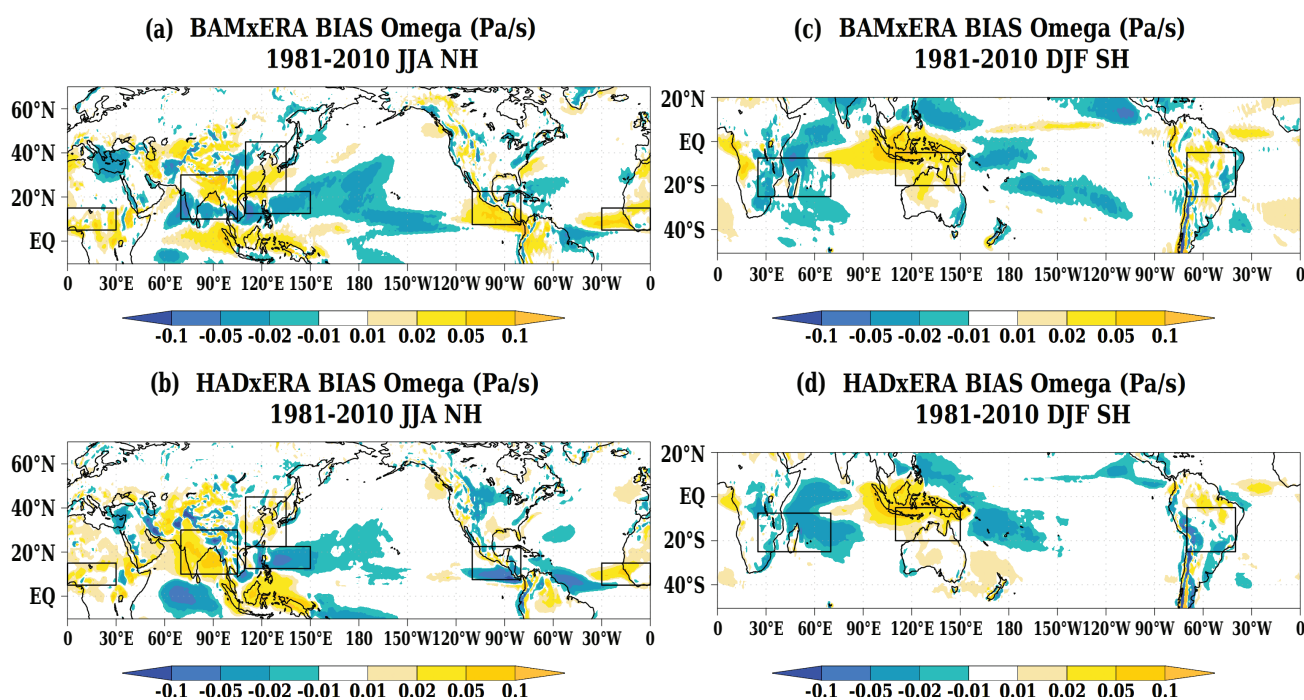


FIGURE 7 Omega bias ( $\text{Pa}\cdot\text{s}^{-1}$ ) calculated between models BAM-v1.2 (a, c), HadGEM3 (b, d) and ERA5. Left panel: NH, right panel: SH. Monsoon areas (black boxes) [Colour figure can be viewed at [wileyonlinelibrary.com](https://onlinelibrary.wiley.com)]

missing air–sea interactions in the model (Zhou *et al.*, 2008; Zou *et al.*, 2016) and the bias of the western Pacific subtropical high (Song and Zhou, 2014b). A comparison between atmospheric models and coupled models of CMIP3 and CMIP5 showed an improvement in the models performance when there are air–sea interactions in the coupled models (Song and Zhou, 2014a; 2014b).

Over India and Bay of Bengal, the two models have opposite behaviour in representing the observed typical summer precipitation pattern. BAM-v1.2 overestimates, while HadGEM3 underestimates precipitation. HadGEM3 underestimates the ascent motion over these regions (i.e., positive omega bias values in Figure 6b), which could explain the negative precipitation bias. Another reason

could be the underestimation of moisture convergence shown in Figures 7c and 8b. Kumar and Sarthi (2021), analysing precipitation in the IMS obtained from four CMIP6 models, concluded that the large variability found among model results could be related to the variations in wind and moisture incursion from the Arabian Sea and Bay of Bengal. The maximum JJA precipitation in Africa, related to humidity from the tropical Atlantic and Indian Ocean, is well simulated by both models, although with a slight negative bias (Figure 5a,b) related to the reduced moisture flux compared to the observation (Figures 7a–c and 8a,b). Raj *et al.* (2019) mention that the ability of a climate model to simulate the NAFMS depends on the representation of the interactions among the main elements of this system, such as the African Easterly Jet, African Easterly Waves, Tropical

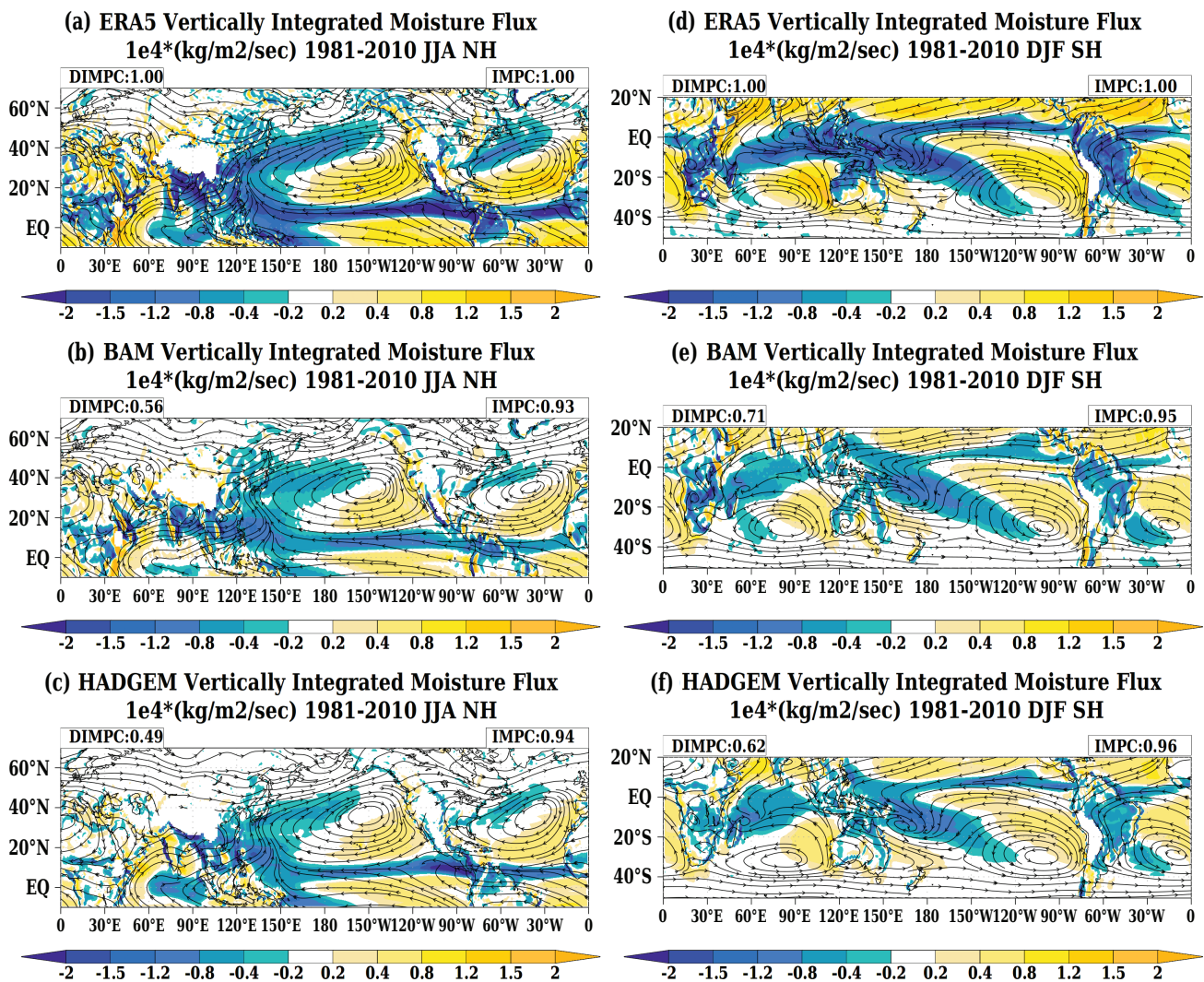


FIGURE 8 Vertically integrated moisture flux divergence ( $10^{-4} \text{ kg} \cdot \text{m}^{-2} \cdot \text{s}^{-1}$ ). ERA5 (top), BAM-v1.2 (middle), HadGEM3 (bottom). Left panel: NH, right panel: SH. The numbers at the upper right corners of each panel are the vertically integrated moisture pattern correlation (IMPC) values computed between the models and ERA5 values shown in these figure panels. The numbers at the upper left corners of each panel are the vertically integrated moisture flux divergence pattern correlation (DIMPC) values computed between the models and observed (GPCP) values shown in these figure panels [Colour figure can be viewed at [wileyonlinelibrary.com](http://wileyonlinelibrary.com)]

Easterly Jet, the Saharan Heat Low and the ITCZ. Then, the precipitation bias could be associated with model deficiencies in representing some of these features, which likely require higher spatial resolutions for producing improved simulations of these elements.

The models also reproduce precipitation in the Central and North America monsoon region, related to the southeasterly flow from the South Atlantic, which crosses northern South America and to the easterly flow from the south branch of the North Atlantic Subtropical High (Figure 4a–c). In the oceanic area of the NAMS, precipitation is underestimated by BAM-v1.2 and overestimated by HadGEM3 (Figure 5a,b). These biases are related to the correspondent underestimation or overestimation of ascent motion (Figure 6a,b) and moisture flux convergence (Figure 8a,b).

In the NH, the common precipitation biases in the two models (Figure 5a,b) are over the Pacific and West Atlantic Oceans (more precipitation than observed), as well as Indonesia (less precipitation than observed). The models have opposite biases in India (wet in BAM-v1.2 and dry in HadGEM3), parts of eastern Asia (dry in BAM-v1.2 and wet in HadGEM3) and east tropical Pacific near Central America (dry in BAM-v1.2 and wet in HadGEM3).

In the SH, the three convergence zones, ICZ, SPCZ and SACZ are captured by the models (Figure 4d–f). The three subtropical anticyclones, at low levels, that bring humidity to the convergence zones are also well

represented by the models. These subtropical highs over South Atlantic, South Pacific and Southern Indian Oceans are very important to the regional climate of the Southern Hemisphere (Cherchi *et al.*, 2018). Although there is a good representation of such anticyclones (high-pressure systems) by the two models, they present a dry bias mainly in the maritime continent region, western coast of Africa and tropical North Atlantic and wet bias mainly in the SPCZ, Africa and Indian Ocean (Figure 5c, d). The maritime continent is located between the Asia and Australia monsoons regions, and precipitation is largely influenced by El Niño–Southern Oscillation (ENSO), Madden–Julian Oscillation (MJO) and complex regional topography (Robertson *et al.*, 2011). This is a very important region from a global perspective, being one of the regions with intense convective activity and therefore a strong heat source for the atmospheric circulation (Neale and Slingo, 2003). Model precipitation errors in this region have been related to the inability of models to reproduce the diurnal precipitation cycle (Neale and Slingo, 2003), deficiencies in convection schemes (Gianotti and Eltahir, 2014), biases in easterly winds and the local Hadley circulation (Toh *et al.*, 2018). A dry bias is also noticed over large areas of South America in BAM-v1.2 while HadGEM3 indicates wet bias in the west and southeast South America. The representation of the SAMS by these two models in the same climate simulation as the present study is detailed in Coelho *et al.* (2021a). Summer precipitation in Australia

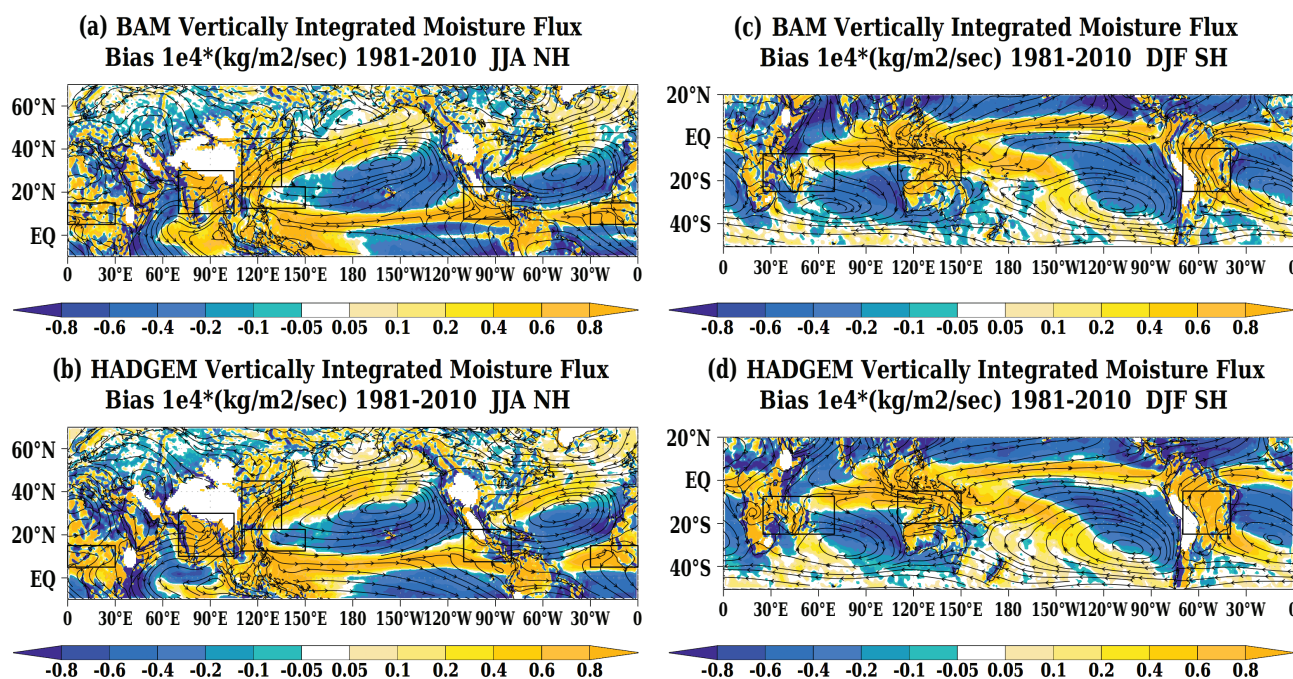
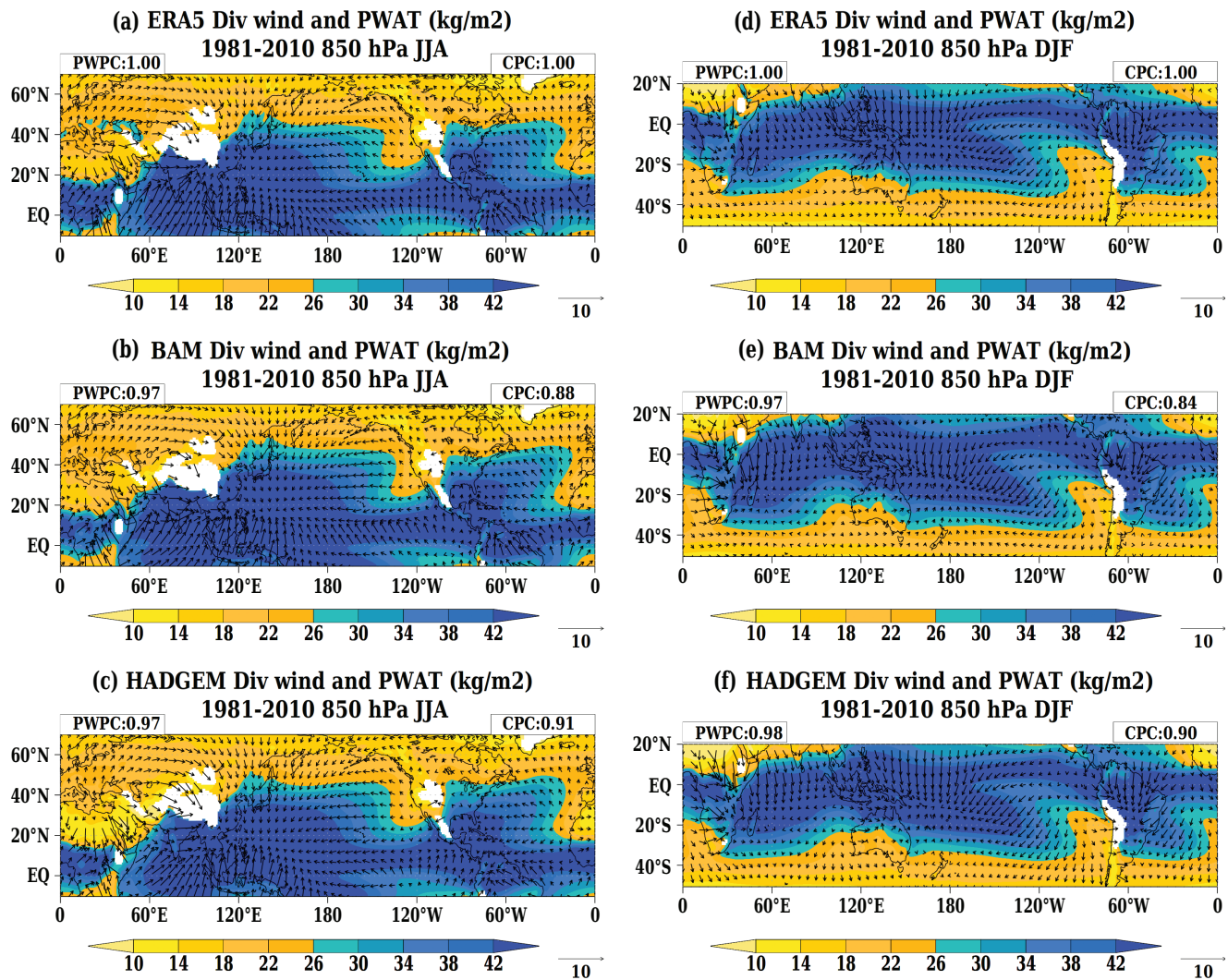


FIGURE 9 Vertically integrated moisture flux divergence bias ( $10^{-4} \text{ kg m}^{-2} \text{ s}^{-1}$ ) calculated between models BAM-v1.2 (a, c), HadGEM3 (b, d) and ERA5. Left panel: NH, right panel: SH. Monsoon areas (black boxes) [Colour figure can be viewed at [wileyonlinelibrary.com](http://wileyonlinelibrary.com)]



**FIGURE 10** Divergent wind ( $\text{m}\cdot\text{s}^{-1}$ ) at 850 hPa and precipitable water (PWAT, shaded,  $\text{kg}\cdot\text{m}^{-1}$ ). ERA5 (top), BAM-v1.2 (middle), HadGEM3 (bottom). Left panel: NH, right panel: SH. The numbers at the upper right corners of each panel are the circulation (divergent wind) pattern correlation (CPC) values computed between the models and ERA5 values. The numbers at the upper left corners of each panel are the precipitable water pattern correlation (PWPC) values computed between the models and ERA5 values [Colour figure can be viewed at [wileyonlinelibrary.com](http://wileyonlinelibrary.com)]

is well simulated, except in the extreme north, with dry bias in both models and a wet bias on the eastern coast by BAM-v1.2. The dry bias in the north is an extension of the reduced precipitation in the maritime continent region. Although there is a dry bias in the maritime continent, this region presents high correlations between observed (GPCP) and models simulated precipitation (Figure 6). The correlations are high over the tropical regions, mainly over the oceans. Over the monsoon regions of India, Eastern Asia and Northwest Pacific the correlations are not statistically significantly different from zero at the 10% level, except in small areas. The statistically significant correlations cover large areas of NAMS and some areas of NAFMS in the NH, and some areas of SAMS, SAFMS and AUSMS in the SH. However,

the precipitation pattern correlations between models and GPCP are 0.93/0.94 (BAM-v1.2/HadGEM3) in the NH and 0.96/0.98 (BAM-v1.2/HadGEM3) in the SH. The 850 hPa circulation pattern correlations are 0.83/0.82 (BAM-v1.2/HadGEM3) in the NH and 0.86/0.87 (BAM-v1.2/HadGEM3) in the SH. At both low and high levels, the precipitation and circulation pattern correlations are a little higher in the SH than in the NH.

The biases in precipitation (Figure 5) are shown to be consistent with biases in vertical motion (Figure 7). The dry bias in the maritime continent region during the NH and SH monsoon seasons corresponds with underestimated ascent, as well as the dry bias in India by HadGEM3 and dry bias in South America in BAM-v1.2. The same occurs in the regions with wet bias, where

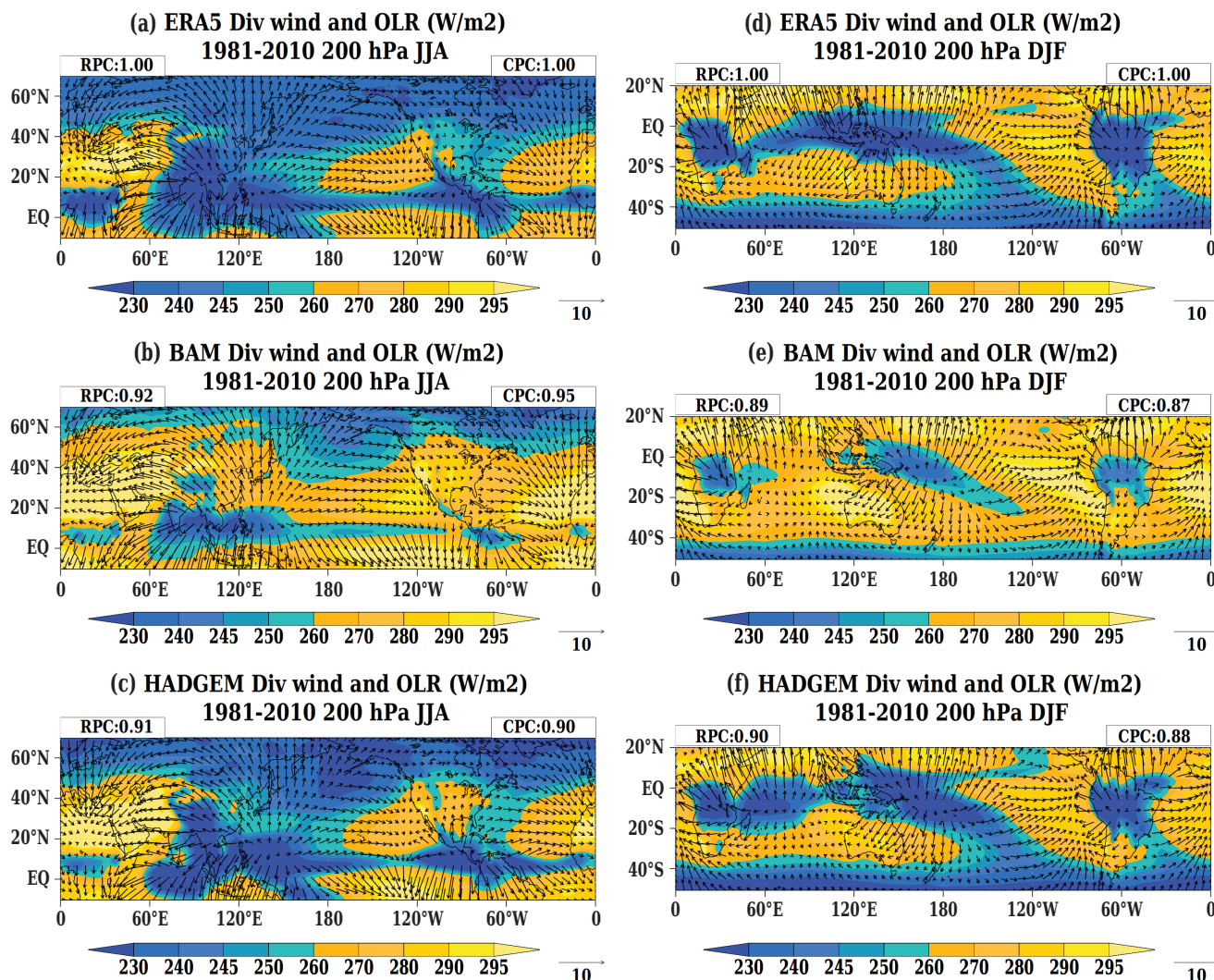


**FIGURE 11** Divergent wind ( $\text{m}\cdot\text{s}^{-1}$ ) at 200 hPa and outgoing longwave radiation (OLR shaded,  $\text{W}\cdot\text{m}^{-2}$ ). ERA5 (top), BAM-v1.2 (middle), HadGEM3 (bottom). Left panel: NH, right panel: SH. The numbers at the upper right corners of each panel are the circulation (divergent wind) pattern correlation (CPC) values computed between the models and ERA5 values. The numbers at the upper left corners of each panel are the outgoing longwave radiation pattern correlation (RPC) values computed between the models and ERA5 values [Colour figure can be viewed at [wileyonlinelibrary.com](http://wileyonlinelibrary.com)]

**TABLE 4** Correlation between monthly precipitation and circulation indices in the period of 1981–2010 for eight monsoon regions

Correlation between precipitation and circulation indices (1981–2010)	GPCP (PREC)_ERA5 (CIRC)	BAM (PREC/CIRC)	HAD (PREC/CIRC)
IMS	0.66	0.72	0.67
WNPMS	0.82	0.86	0.81
EAMS	0.71	0.73	0.83
NAMS	0.86	0.83	0.87
NAFMS	0.72	0.67	0.65
SAFMS	0.71	0.76	0.74
SAMS	0.71	0.65	0.67
AUSMS	0.85	0.70	0.68

Note: For the NH (SH) the analysis includes June, July and August (December, January and February) values. Observation (GPCP and ERA5), BAM-v1.2 and HadGEM3 models.

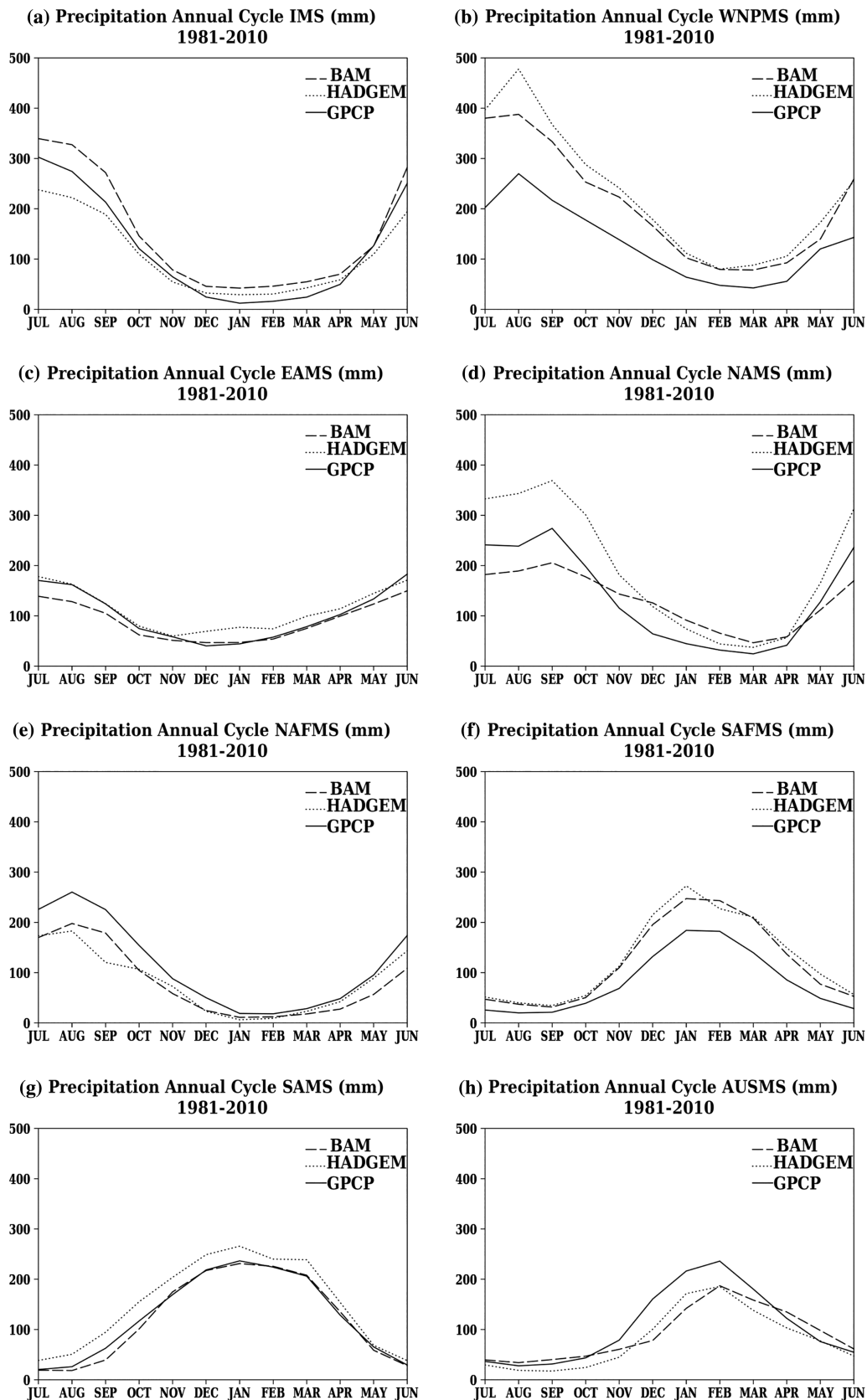
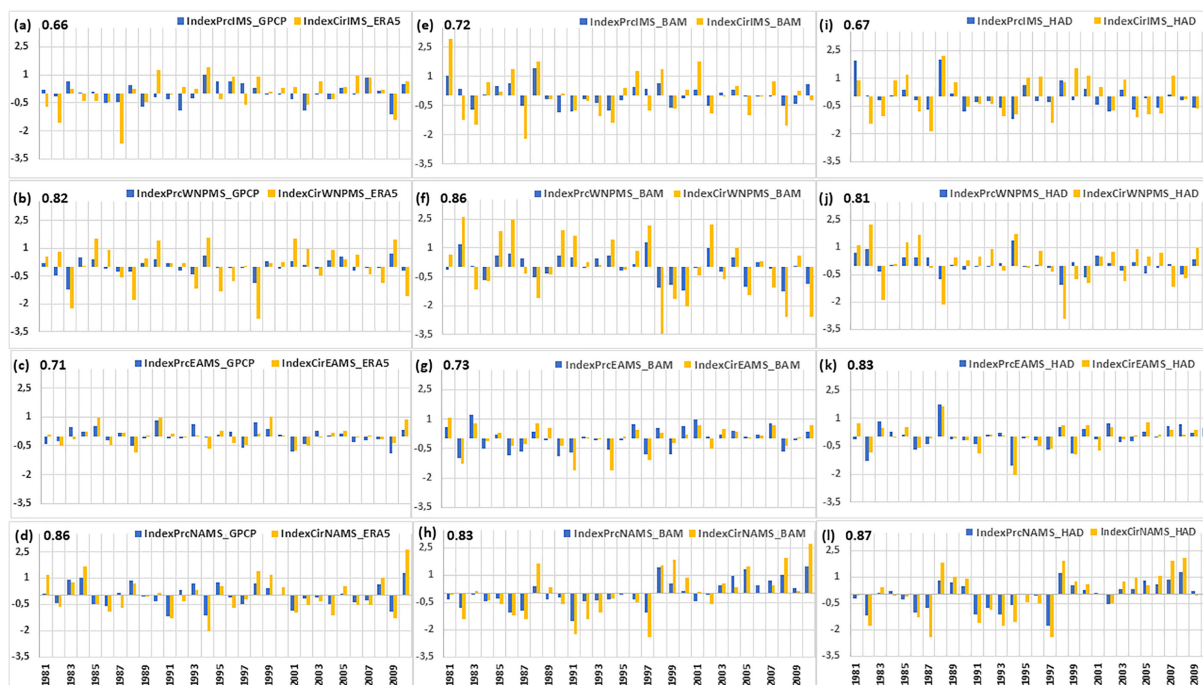
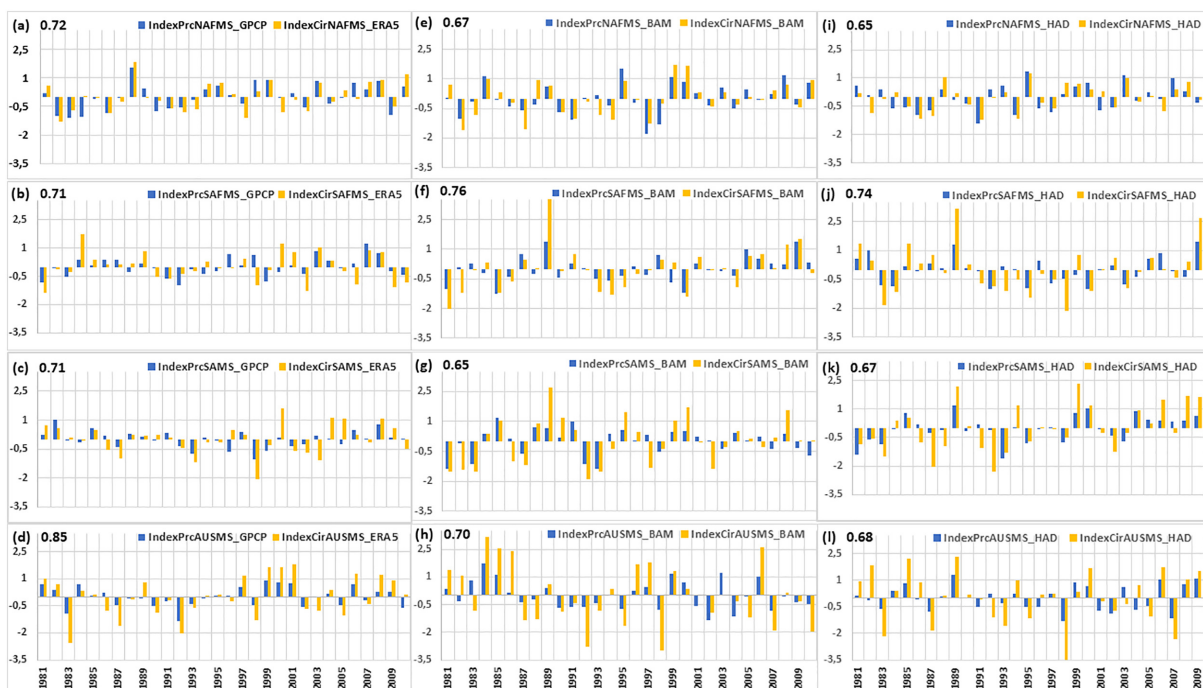


FIGURE 12 Annual cycle of mean precipitation (mm), calculated as an average of precipitation in the regions of Figure 1 and Table 1



**FIGURE 13** Timeseries of precipitation index (blue) and circulation index (red) calculated from observational data and model simulations. Observational: (a) IMS, (b) NWPMS, (c) EAMS, (d) NAMS; BAM-v1.2: (e) IMS, (f) NWPMS, (g) EAMS, (h) NAMS; HadGEM3: (i) IMS, (j) NWPMS, (k) EAMS, (l) NAMS. Numbers in the upper left corner are correlations between monthly precipitation and circulation indices in the period of 1981–2010 for each monsoon region [Colour figure can be viewed at [wileyonlinelibrary.com](http://wileyonlinelibrary.com)]



**FIGURE 14** Timeseries of precipitation index (blue) and circulation index (red) calculated from observational data and model simulations. Observational: (a) NAFMS, (b) SAFMS, (c) SAMS, (d) AUSMS; BAM-v1.2: (e) NAFMS, (f) SAFMS, (g) SAMS, (h) AUSMS; HadGEM3: (i) NAFMS, (j) SAFMS, (k) SAMS, (l) AUSMS. Numbers in the upper left corner are correlations between monthly precipitation and circulation indices in the period of 1981–2010 for each monsoon region [Colour figure can be viewed at [wileyonlinelibrary.com](http://wileyonlinelibrary.com)]

ascent is overestimated. The precipitation biases are also associated with biases in the vertically integrated humidity flux (Figure 9). Although the general humidity flux patterns are well represented (Figure 8), the moisture convergence is underestimated, mainly in the maritime continent region and South America, and overestimated over Pacific and Indian Oceans. The underestimation of moisture convergence in IMS by HadGEM3 is consistent with the precipitation underestimation in that region. The vertically integrated moisture flux pattern correlations between model simulations and ERA5 are 0.93/0.94 (BAM-v1.2/HadGEM3) in the NH and 0.95/0.96 (BAM-v1.2/HadGEM3) in the SH. The vertically integrated moisture flux divergence pattern correlations are lower: 0.56/0.49 (BAM-v1.2/HadGEM3) in the NH and 0.71/0.62 (BAM-v1.2/HadGEM3) in the SH.

Besides the common features of maximum summer precipitation, ascending motion and humidity flux in the monsoon regions, there is convergence at low levels (Figure 10a,d) and divergence at high levels (Figure 11a,

d), shown by divergent winds. The convergence at low levels and divergence at high levels, as well as the anticyclonic circulation at high levels are basic features of the monsoon regions (Chen, 2003). These features are well captured by the two models (Figures 10b,c,e,f and 11b,c,e,f). The low levels divergent wind pattern correlations between models and ERA5 are 0.88/0.91 (BAM-v1.2/HadGEM3) in the NH and 0.84/0.90 (BAM-v1.2/HadGEM3) in the SH. At high levels, the divergent wind pattern correlation are 0.95/0.90 (BAMv1.2/HadGEM3) in the NH and 0.87/0.88 (BAM-v1.2/HadGEM3) in the SH. Precipitable water, which is shown in Figure 10, is also well simulated by the two models. The precipitable water patterns correlations between models and ERA5 are 0.97 for both models in the NH and 0.97/0.98 (BAM-v1.2/HadGEM3) in the SH.

OLR presented in Figure 11 shows a similar observed convection configuration in HadGEM3 (Figure 11c,f), but higher than observed OLR in BAM-v1.2, which means reduced convection in the monsoon regions (Figure 11b,

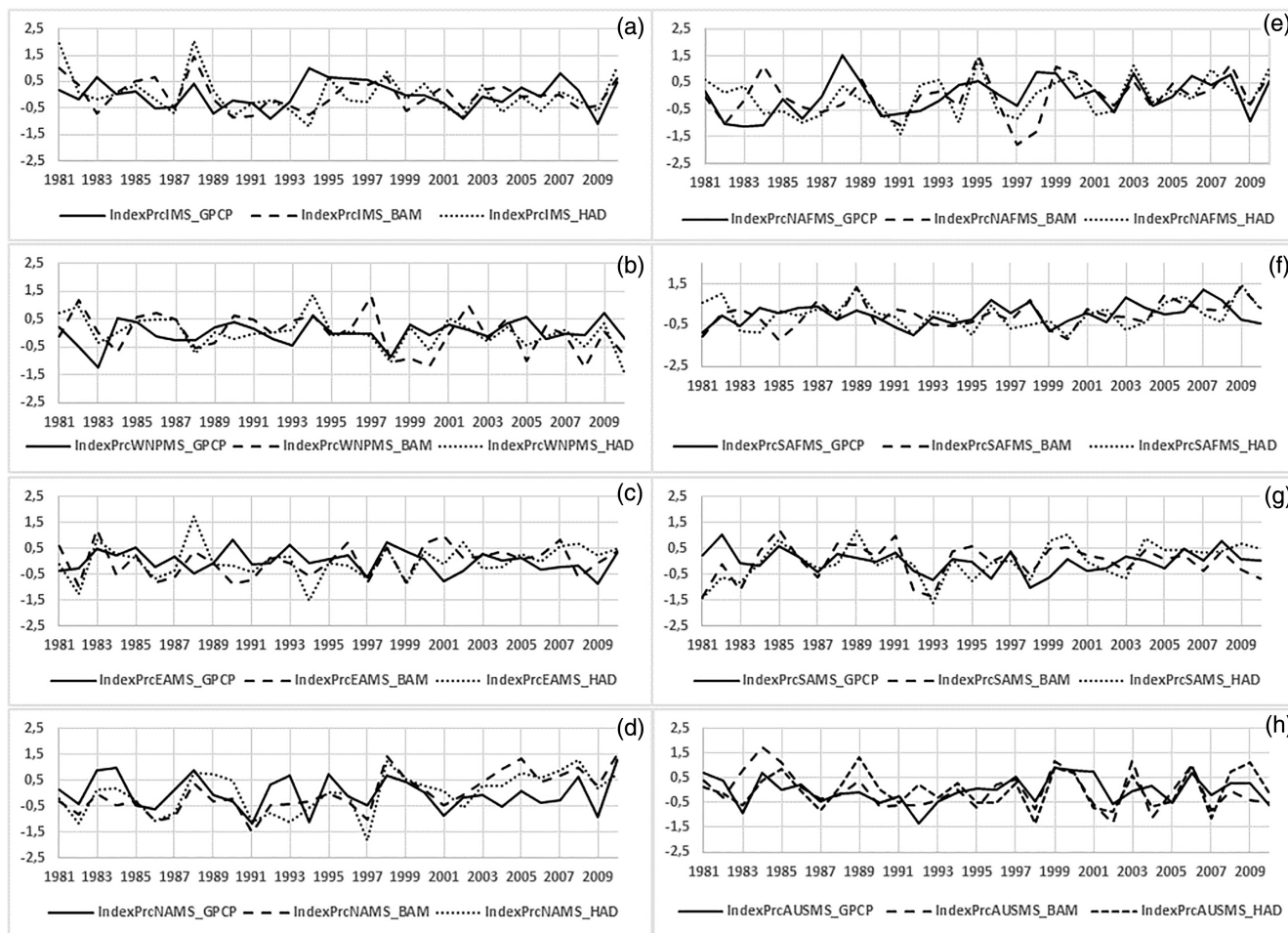


FIGURE 15 Timeseries of precipitation index calculated from observational data and model simulations (BAM-v1.2 and HadGEM3) for eight monsoon regions. (a) IMS, (b) NWPMS, (c) EAMS, (d) NAMS; (e) NAFMS, (f) SAFMS, (g) SAMS, (h) AUSMS

e). The highest OLR values in the regions of the subtropical highs, Northern Africa and Australia, are overestimated by BAM-v1.2, while HadGEM3 overestimates in Northern Africa during NH summer. This OLR overestimation in BAM-v1.2 is related to deficiencies in cloud–radiation interactions, as mentioned above (Coelho *et al.*, 2021a; 2021b). OLR pattern correlations between models and NOAA data are 0.92/0.91 (BAM-v1.2/HadGEM3) in the NH and 0.89/0.90 (BAM-v1.2/HadGEM3) in the SH.

#### 4 | ANNUAL CYCLE AND MONSOON INDICES

The two models represent the annual cycle of the PI for the eight monsoon areas, listed in Table 4, reasonably well (Figure 12). However, they overestimate the precipitation in WNPMS (Figure 12b) and SAFMS (Figure 12f), and underestimate in NAFMS (Figure 12e) during the

whole year. In AUSMS (Figure 12h), both models underestimate during the austral warm season. BAM-v1.2 adequately simulates the annual cycle in SAMS, while HadGEM3 overestimates it (Figure 12g). The common feature of all monsoon regions is the precipitation contrast between summer and winter, unless the EAMS, which shows smaller differences (Figure 12c).

In the monsoon regions, precipitation has a strong association with wind flow at low levels, as this flow brings humidity from the ocean to the continent in the summer season. In order to verify how well, in the models, precipitation is related to atmospheric circulation in each monsoon region, correlations between their indices, specified in section 2 were calculated. The precipitation and circulation indices obtained from ERA-5 (circulation) and GPCP (precipitation) are well correlated in all monsoon regions, with values from 0.66 to 0.86 for the period of 1981–2010 (Table 3). The highest correlations are noticed in NAMS, AUSMS and WNPMS. The models present a correlation between the two indices similar to the observed indices for

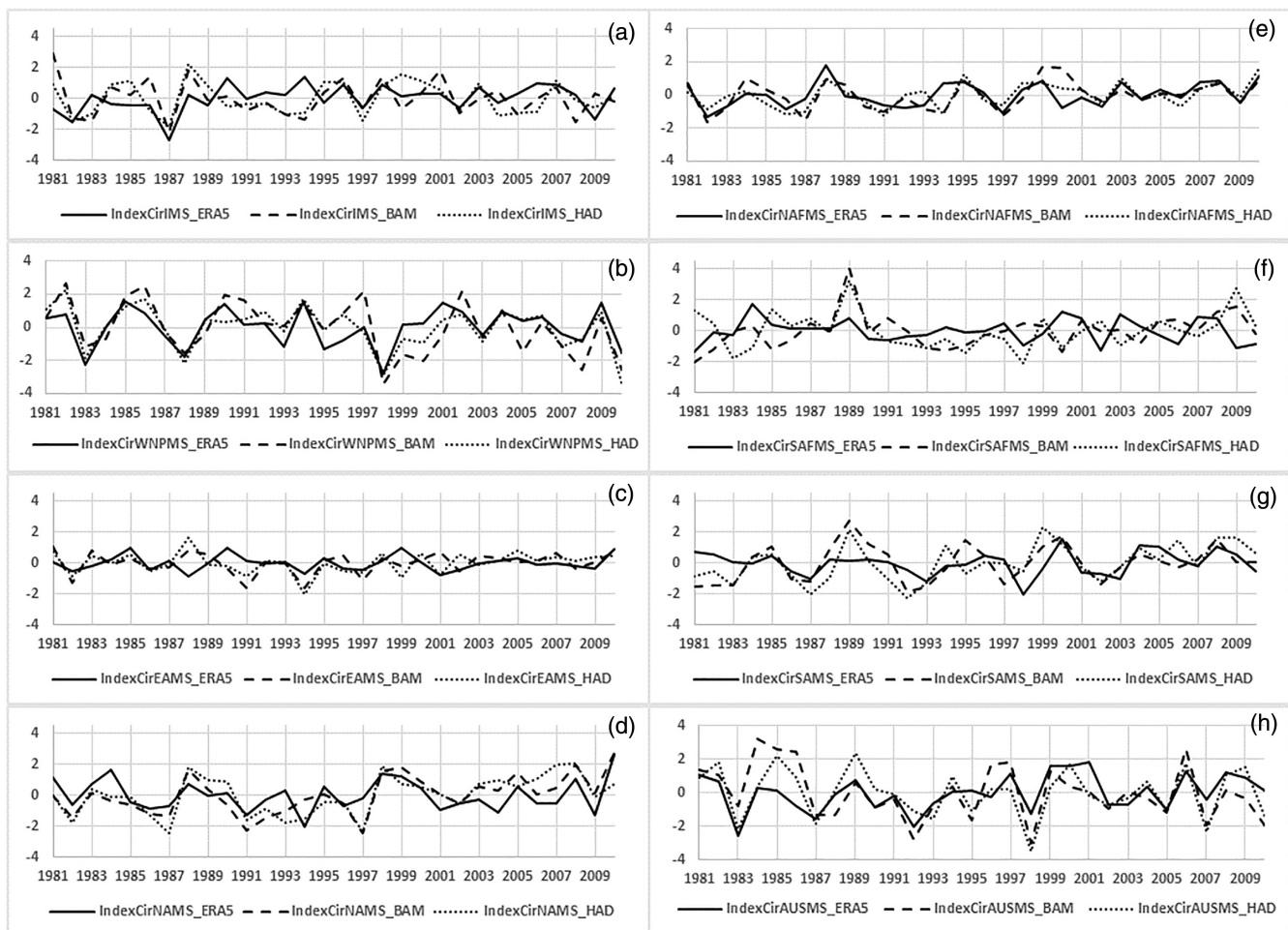


**FIGURE 16** Timeseries of circulation index calculated from observational data and model simulations (BAM-v1.2 and HadGEM3) for eight monsoon regions. (a) IMS, (b) WNPMS, (c) EAMS, (d) NAMS; (e) NAFMS, (f) SAFMS, (g) SAMS, (h) AUSMS

**TABLE 5** Correlation between precipitation and circulation indices calculated by averaging the monthly values over each summer season over the 1981–2010 period for eight monsoon regions between models (BAM-v1.2 and HadGEM3) and Observations (GPCP and ERA5)

Monsoon regions	1981–2010			
	Correlation between precipitation indices BAM and HAD vs. GPCP		Correlation between circulation indices BAM and HAD vs. ERA5	
	PREC_BAMxGPCP	PREC_HADxGPCP	CIRC_BAMxERA5	CIRC_HADxERA5
Correl_index_IMS	0.19	<b>0.31</b>	0.20	0.32
Correl_index_WNPMS	0.03	<b>0.39</b>	<b>0.66</b>	<b>0.81</b>
Correl_index_EAMS	−0.01	0.03	0.14	0.12
Correl_index_NAMS	<b>0.44</b>	<b>0.39</b>	<b>0.60</b>	<b>0.44</b>
Correl_index_NAFMS	<b>0.32</b>	<b>0.44</b>	<b>0.58</b>	<b>0.66</b>
Correl_index_SAFMS	0.26	0.02	0.10	−0.16
Correl_index_SAMS	<b>0.37</b>	0.24	<b>0.40</b>	<b>0.44</b>
Correl_index_AUSMS	<b>0.46</b>	<b>0.42</b>	<b>0.52</b>	<b>0.66</b>

Note: Correlation values above 0.31 (values in bold) are statistically significant using the *t* test for correlation at the 10% level ( $t > 1.701$  and  $< -1.701$ )

the regions of NWPMS, NAMS and SAFMS. The correlations in SAMS, AUSMS, NAFMS are lower in the models than in the observations, and in EAMS, BAM-v1.2 shows similar correlations, while HadGEM3 has higher values than observed. On the contrary, in IMS, HadGEM3 presents similar values, and BAM-v1.2 shows higher correlations than observed.

Timeseries of the two indices calculated by averaging the monthly values over each summer season during 1981–2010 in the eight monsoon regions are plotted in Figures 13 and 14. This analysis is similar to Wang and He (2019). It is seen that these two indices have a marked interannual variability, in both intensity and sign. In many years the two models represent the indices with the same signal, similar to the observations, although with different intensities. Then, in the majority of regions, the models can identify the relationship between circulation and precipitation. The highest circulation indices observed in WNPMS (Figure 13b,f,j) are captured by both models, as well as the low intensities of precipitation and circulation indices in EAMS (Figure 13c,g,k). Timeseries of precipitation and circulation indices calculated by averaging the monthly values over each summer season during 1981–2010 for both models and GPCP are shown in Figures 15 and 16. The interannual variability of precipitation is captured by the models in some years, but the correlations between each model (BAM-v1.2/HadGEM3) and GPCP series in Table 5 are statistically significant different from zero at the 10% level only in NAMS (0.44/0.39), NAFMS (0.32/0.44) and AUSMS (0.46/0.42). In IMS and WNPMS, only HadGEM3 shows statistically significant correlations of 0.31 and 0.39,

respectively, while in SAMS, only BAM-v1.2 presents significant correlation of 0.37.

For IMS, the two models present similar precipitation variability or similar values to observations in 1982, 1985, 1987, 1988, 1989, 1993, 2002, 2003, 2009 and 2010 (Figure 15a). For WNPMS, the similar variability or similar values are identified in 1983, 1985, 1994, 1995, 1998, 2003, 2004, 2007, 2009 and 2010 (Figure 15b). EAMS presents similar variability or similar values in 1983, 1986, 1989, 1992, 1994, 1997, 1998, 2000, 2003, 2005 and 2010 (Figure 15c). Similar variability or similar values in NAMS occur in 1982, 1983, 1985, 1988, 1991, 1992, 1997, 1998, 1999, 2000, 2001, 2002, 2005, 2006, 2008, 2009 and 2010 (Figure 15d). NAFMS shows similar variability or similar values in 1990, 1997, 1998, 2002, 2003, 2004, 2005, 2009 and 2010 (Figure 15e). The timeseries of observation and model precipitation in SAFMS indicate similar variability or similar values in 1988, 1996, 1997 and 2001 (Figure 15f). For SAMS, similar variability or similar values occur in 1982, 1985, 1986, 1987, 1991, 1993, 1994, 1998 and 1999 (Figure 15g). For AUSMS the similar variability or similar values occur in 1986, 1987, 1993, 1994, 1997, 1998, 1999, 2000, 2002, 2006, 2007 and 2008 (Figure 15h).

The circulation indices have more cases of similar variability or similar values (Figure 16) and the statistically significant correlations in Table 4, between each model (BAM-v1.2/HadGEM3) and ERA5 occur in WNPMS (0.66/0.81), NAMS (0.60/0.44), NAFMS (0.58/0.66), SAMS (0.40/0.44) and AUSMS (0.52/0.66). It is worth to emphasize that the correlations are higher for circulation indices than for precipitation, showing the better ability of models in representing circulation. Similar circulation indices were

analysed by Zhou *et al.* (2009b) in the Asia-Australian region, using a multimodel set of atmospheric simulations, discussing the role of SST on circulation.

## 5 | DISCUSSION AND CONCLUSION

This study evaluated the representation of monsoons features in climate simulations of two global atmospheric models: BAM-v1.2 and HadGEM3. The period of analyses was 1981–2010, and the results were compared to ERA5 reanalysis and GPCP dataset. Observed global monsoon characteristics were identified in the simulations from both models. The spatial extent of the NH and the SH monsoon domains were reproduced by the models, as well as the summer characteristics of atmospheric circulation at low and high levels. The models' precipitation in the monsoon regions displayed similar features to observations, although there were biases in some areas, mainly in the maritime continent (dry) and Pacific and Indian Oceans (wet). In the EAMS region, the models presented opposite precipitation biases: dry in BAM-v.1 and wet in HadGEM3. On the contrary, the IMS region displayed wet bias in BAM-v.1 and dry in HadGEM3. The models also showed opposite precipitation bias in the NAMS region: dry in BAM-v.1 and wet in HadGEM3. In the SAMS region, both models indicated dry biases over parts of Amazon and wet biases in parts of Southeast Brazil. The two models also represented similar biases in the SAFMS: wet bias over eastern and dry bias over parts of western South Africa. In the NAFMS region the both models showed a dry bias in parts of the domain. A dry bias in the AUSMS was also exhibited in both models. Biases in these regions are related to errors in ascending motion and humidity flux.

The present analyses showed that the main features of the global monsoon were represented by the two models, BAMv1.2 and HadGEM3. However, there was an overestimation or underestimation of some variables, indicating errors in their intensities. Common features of the monsoon regions were high-level anticyclones, low-level inland flow, ascending vertical motion, humidity flux to the continents, divergence at high levels and convergence at low levels, the annual cycle of precipitation and relations between precipitation and circulation. These common features were adequately represented by the models, except the Mexican High at high levels that was not well organized in the HadGEM3 model. In each hemisphere, the global precipitation and circulation showed features of the monsoon systems, which were reproduced by the models. Considering the annual cycle of precipitation, in the NH, the larger errors were found

in the WNPMS and NAMS, while in the IMS, EAMS and NAFMS, the annual cycles of precipitation were close to observations. In the SH, the annual cycles followed the observations, mainly in the SAMS, with overestimation in the SAFMS and underestimation in the AUSMS. In the majority of years the models reproduced the relationship between precipitation and circulation indices, with high association measured by computing the correlations between the times series of these two indices. However, the correlations between models precipitation indices and GPCP were low and only statistically significant at the 10% level in NAMS, NAFMS, AUSMS (BAM-v1.2 and HadGEM3), in IMS and WNPMS (HadGEM3), and in SAMS (BAM-v1.2). The circulation index presented higher correlation values between models and ERA5, with significantly significant values in WNPMS, NAMS, NAFMS, SAMS, AUSMS (BAM-v1.2 and HadGEM3) and in IMS (HadGEM3).

The models' performance are affected by the lack of ocean–atmosphere interaction but also by deficiencies in the representation of physical processes. Good *et al.* (2021) report that tropical precipitation sensitivity to local SSTs is too weak in CMIP5 models, contributing to model precipitation and circulation biases. The authors suggest that the response of shallow precipitating convection to SST variation could be important for improving these biases. BAM1.2 and HadGEM3 AMIP simulations used in this study are driven with observed SSTs, but if the models do not properly represent precipitation–SST coupling then this could contribute to the biases in monsoon representation reported in this study.

In addition, errors in precipitation over the continents may be related to errors in humidity flux, humidity convergence and vertical motion, as identified in the present study. The role of vertical motion and water vapour on precipitation bias was discussed in Yang *et al.* (2018), with analyses of four CMIP5 models. John and Soden (2007) analysed water vapour in global climate models simulations and found, in its majority, a dry bias in the boundary layer and a larger wet bias in the free atmosphere. However, as the planetary boundary layer (PBL) is relevant for the vertical transport of heat, moisture, momentum and other physical proprieties (Garrat, 1994) a good parameterization can reduce amplification of errors. Other parameterizations, like radiation and convection need to be better adjusted in the models, to reduce errors.

The atmospheric moisture flux divergence bias, noticed in the results, may be related to errors in soil moisture–atmosphere interactions and to the horizontal advection of moisture in the free atmosphere. The soil moisture coupling with atmospheric variables and representation by models was discussed in Koster *et al.* (2004) and Seneviratne *et al.*

(2010). They identified, in the Global Land-Atmosphere Coupling Experiment (GLACE), hot spots of soil moisture–temperature and soil moisture–precipitation couplings in regions of North America, India and northern Africa. For Eastern Asia there was only coupling between soil moisture and temperature. The results were obtained by a multi-model analysis, but there was large variability among the 12 models. Thus, the inability of models to represent these couplings can propagate errors in the hydrological cycle. The role of wind biases of CMIP6 models on moisture advection was discussed in Baker and Spracklen (2022) when analysing rainfall recycling in Amazon and Congo basins. Although BAM-v1.2 and HadGEM3 represent large-scale convergence at low levels and divergence at high levels relatively well, moisture flux biases need to be investigated in the light of existing wind and evaporation biases.

Model resolution can also be a source of errors. Demory *et al.* (2014) evaluated the impact of changing horizontal resolution in HadGEM3 on model representation of the hydrological cycle. In general, they found that biases in radiation result in biases in the hydrological cycle, with too much moisture being transported from the ocean onto land. Furthermore, representation of precipitation in the models was sensitive to horizontal resolution, with precipitation decreasing over the oceans with increasing model resolution (i.e., becoming closer to observations) and increasing over land (further away from observations). Mitra (2021) assessed representation of the Indian monsoon in CMIP6 models and observed that models generally overestimate the spatial coherence of monsoon rainfall. The models simulated large-scale, spatially homogenous rain events spanning several grid cells, missing the heterogeneity present in observations. Thus, this is further evidence that the coarse horizontal resolution of HadGEM3 and BAM1.2 could contribute to monsoon biases shown in our study.

In this study, the identification of deficiencies in humidity flux, omega and OLR, related to precipitation in monsoon regions, suggests the importance of continuous development of these models, both in the dynamical core and parameterizations of convection, radiation and PBL, aiming to reduce errors and improve the quality of the produced simulations.

## ACKNOWLEDGEMENTS

To Fundação de Amparo à Pesquisa do Estado de São Paulo (FAPESP)-Belmont Forum-CLIMAX-2015/50687-8 and Coordenação de Aperfeiçoamento de Pessoal de Nível Superior (CAPES) 88887145932/2017-01. IFAC thanks Conselho Nacional de Desenvolvimento Científico e Tecnológico (CNPq) project 306393/2018-2, CASC thanks CNPq, project 305206/2019-2 and DCS was supported by CAPES project 88887.469114/2019-00. We also thank the two anonymous reviewers for providing valuable comments

and suggestions that contributed to improving the quality of this manuscript.

## DATA AVAILABILITY STATEMENT

ERA-5 reanalysis data used in this study are available at <https://cds.climate.copernicus.eu/cdsapp#!/dataset/reanalysis-era5-pressure-levels-monthly-means?tab=overview> and <https://cds.climate.copernicus.eu/cdsapp#!/dataset/reanalysis-era5-single-levels-monthly-means?tab=overview>. GPCP v2.3 data used in this study are available at <https://www.ncei.noaa.gov/data/global-precipitation-climatology-project-gpcp-monthly/access/>. OLR is provided by NOAA/NCEP.

## ORCID

Iracema F. A. Cavalcanti  <https://orcid.org/0000-0002-3890-5767>

Caio A. S. Coelho  <https://orcid.org/0000-0002-9695-5113>

## REFERENCES

- Adler, R.F., Huffman, G.J., Chang, A., Ferraro, R., Xie, P., Janowiak, J., McNab, A., Rudolf, B. and Schneider, U. (2003) The version 2 Global Precipitation Climatology Project (GPCP) monthly precipitation analysis (1979–present). *Journal of Hydrometeorology*, 4, 1147–1167.
- Baker, J.C.A., Castilho de Souza, D., Kubota, P.Y., Buermann, W., Coelho, C.A.S., Andrews, M.B., Gloor, M., Garcia-Carreras, L., Figueroa, S.N. and Spracklen, D.V. (2021) An assessment of land–atmosphere interactions over South America using satellites, reanalysis, and two global climate models. *Journal of Hydrometeorology*, 22, 905–922.
- Baker, J.C.A. and Spracklen, D.V. (2022) Divergent representation of precipitation recycling in the Amazon and Congo in CMIP6 models. *Geophysical Research Letters*, 49, e2021GL095136.
- Barbosa, H.M.J., Tarasova, T.A. and Cavalcanti, I.F.A. (2008) Impacts of a new solar radiation parameterization on the CPTEC AGCM climatological features. *Journal of Applied Meteorology and Climatology*, 47, 1377–1392. <https://doi.org/10.1175/2007JAMC1760.1>.
- Boo, K.O., Martin, G., Sellar, A., Senior, C. and Byun, Y.H. (2011) Evaluating the East Asian monsoon simulation in climate models. *Journal of Geophysical Research: Atmospheres*, 116, 1–13. <https://doi.org/10.1029/2010JD014737>.
- Bretherton, C.S. and Park, S. (2009) A new moist turbulence parameterization in the community atmosphere model. *Journal of Climate*, 22, 3422–3448.
- Carvalho, L.M.V. and Cavalcanti, I.F.A. (2016) The South American monsoon system. In: Carvalho, L.M.V. and Jones, C. (Eds.) *The Monsoons and Climate Change*. Switzerland: Springer International Publishing, pp. 121–148.
- Cavalcanti, I.F.A. and Raia, A. (2017) Lifecycle of South American monsoon system simulated by CPTEC/INPE AGCM. *International Journal of Climatology*, 37, 878–896. <https://doi.org/10.1002/joc.5044>.
- Cavalcanti, I.F.A., Silveira, V.P., Figueroa, S.N., Kubota, P.Y., Bonatti, J.P. and de Souza, D.C. (2020) Climate variability over

- South America—regional and large scale features simulated by the Brazilian Atmospheric Model (BAM-v0). *International Journal of Climatology*, 40, 2845–2869.
- Chen, T.-C. (2003) Maintenance of summer monsoon circulations: a planetary-scale perspective. *Journal of Climate*, 16, 2022–2037.
- Chen, Z., Zhou, T., Zhang, L., Chen, X., Zhang, W. and Jiang, J. (2020) Global land monsoon precipitation changes in CMIP6 projections. *Geophysical Research Letters*, 47, e2019GL086902.
- Cherchi, A., Ambrizzi, T., Behera, S., Freitas, A.C.V., Morioka, T. and Zhou, T. (2018) The response of subtropical highs to climate change. *Current Climate Change Reports*, 4, 371–382. <https://doi.org/10.1007/s40641-018-0114-1>.
- Chou, M.D. and Suarez, M.J. (1999) A solar radiation parameterization (CLRAD-SW) for atmospheric studies. In: Suarez, M.J. (Ed.) *Technical Report Series on global modeling and data assimilation*, Vol. 15. Goddard Space Flight Center Greenbelt, MD: Climate and Radiation Branch Goddard Space Flight Center.
- Chou, M.D., Suarez, M.J., Liang, X.Z., Yan, M.M. and Cote, C. (2001) *A thermal infrared radiation parameterization for atmospheric studies*, Vol. 19. Goddard Space Flight Center Greenbelt, MD: Climate and Radiation Branch Goddard Space Flight Center. Available at: <https://ntrs.nasa.gov/citations/20010072848>.
- Coelho, C.A.S., de Souza, D.C., Kubota, P.Y., Cavalcanti, I.F.A., Baker, J.C.A., Figueroa, S.N., Firpo, M.A.F., Guimarães, B.S., Costa, S.M.S., Gonçalves, L.J.M., Bonatti, J.P., Sampaio, G., Klingaman, N.P., Chevuturi, A. and Andrews, M.B. (2021a) Assessing the representation of South American monsoon features in Brazil and UK climate model simulations. *Climate Resilience and Sustainability*, 1, e27. <https://doi.org/10.1002/cli2.27>.
- Coelho, C.A.S., de Souza, D.C., Kubota, P.Y., Costa, S.M.S., Menezes, L., Guimarães, B.S., Figueroa, S.N., Bonatti, J.P., Cavalcanti, I.F.A., Sampaio, G., Klingaman, N.P. and Baker, J.C.A. (2021b) Evaluation of climate simulations produced with the Brazilian global atmospheric model version 1.2. *Climate Dynamics*, 56, 873–898. <https://doi.org/10.1007/s00382-020-05508-8>.
- Colman, R.A., Moise, A.F. and Hanson, L.I. (2011) Tropical Australian climate and the Australian monsoon as simulated by 23 CMIP3 models. *Journal of Geophysical Research*, 116, D10116. <https://doi.org/10.1029/2010JD015149>.
- Demory, M.E., Vidale, P.L., Roberts, M.J., Berrisford, P., Strachan, J., Schiemann, R. and Mizielinski, M.S. (2014) The role of horizontal resolution in simulating drivers of the global hydrological cycle. *Climate Dynamics*, 42, 2201–2225. <https://doi.org/10.1007/s00382-013-1924-4>.
- Ebert, E.E. and Curry, J.A. (1992) A parameterization of ice cloud optical properties for climate models. *Journal of Geophysical Research*, 97, 3831–3836.
- Figueroa, S.N., Bonatti, J.P., Kubota, P.Y., Grell, G.A., Morrison, H., Barros, S.R.M., Fernandez, J.P.R., Ramirez, E., Siqueira, L., Luzia, G., Silva, J., Silva, J.R., Pendaharkar, J., Capistrano, V.B., Alvim, D.S., Enoré, D.P., Diniz, F.L.R., Satyamurti, P., Cavalcanti, I.F.A., Nobre, P., Barbosa, H.M.J., Mendes, C.L. and Panetta, J. (2016) The Brazilian global atmospheric model (BAM): performance for tropical rainfall forecasting and sensitivity to convective scheme and horizontal resolution. *Weather and Forecasting*, 31, 1547–1572.
- García-Franco, J.L., Gray, L.J. and Osprey, S. (2020) The American monsoon system in HadGEM3 and UKESM1. *Weather Climate Dynamics*, 1, 349–371. <https://doi.org/10.5194/wcd-1-349-2020>.
- Garrat, J.R. (1994) Review: the atmospheric boundary layer. *Earth Science Reviews*, 37, 89–134.
- Gianotti, R.L. and Eltahir, E.A.B. (2014) Regional climate modeling over the maritime continent. Part II: new parameterization for autoconversion of convective rainfall. *Journal of Climate*, 27, 1504–1523. <https://doi.org/10.1175/JCLI-D-13-00171.1>.
- Good, P., Chadwick, R., Holloway, C.E., Kennedy, J., Lowe, J.A., Roehrig, R. and Rushley, S.S. (2021) High sensitivity of tropical precipitation to local sea surface temperature. *Nature*, 589, 408–414.
- Han, J. and Pan, H.L. (2011) Revision of convection and vertical diffusion schemes in the NCEP global forecast system. *Weather and Forecasting*, 26, 520–533.
- Hannak, L., Knippertz, P., Fink, A.H., Kniffka, A. and Pante, G. (2017) Why do global climate models struggle to represent low-level clouds in the West African summer monsoon? *Journal of Climate*, 30, 1665–1687. <https://doi.org/10.1175/JCLI-D-16-0451.1>.
- Hersbach, H., Bell, B., Berrisford, P., Hirahara, S., Horányi, A., Muñoz-Sabater, J., Nicolas, J., Peubey, C., Radu, R., Schepers, D., Simmons, A., Soci, C., Abdalla, S., Abellan, X., Balsamo, G., Bechtold, P., Biavati, G., Bidlot, J., Bonavita, M., De Chiara, G., Dahlgren, P., Dee, D., Diamantakis, M., Dragani, R., Flemming, J., Forbes, R., Fuentes, M., Geer, A., Haimberger, L., Healy, S., Hogan, R.J., Hólm, E., Janisková, M., Keeley, S., Laloyaux, P., Lopez, P., Lupu, C., Radnoti, G., Rosnay, P., Rozum, I., Vamborg, F., Villaume, S. and Thépaut, J.-N. (2020) The ERA5 global reanalysis. *Quarterly Journal of the Royal Meteorological Society*, 146, 1999–2049.
- Hsu, P., Li, T., Murakami, H. and Kitoh, A. (2013) Future change of the global monsoon revealed from 19 CMIP5 models. *Journal of Geophysical Research: Atmospheres*, 118, 1247–1260. <https://doi.org/10.1002/JGRD.50145>.
- Huang, F., Xu, Z. and Guo, W. (2019) Evaluating vector winds in the Asian-Australian monsoon region simulated by 37 CMIP5 models. *Climate Dynamics*, 53, 491–507. <https://doi.org/10.1007/s00382-018-4599-z>.
- Jain, S., Salunke, P., Mishra, S.K. and Sahany, S. (2018) Performance of CMIP5 models in the simulation of Indian summer monsoon. *Theoretical and Applied Climatology*, 137, 1429–1447.
- John, V.O. and Soden, B.J. (2007) Temperature and humidity biases in global climate models and their impact on climate feedbacks. *Geophysical Research Letters*, 34, L18704.
- Kim, H.J., Wang, B. and Ding, Q. (2008) The global monsoon variability simulated by CMIP3 coupled climate models. *Journal of Climate*, 21, 5271–5294.
- Kitoh, A., Endo, H., Kumar, K.K., Cavalcanti, I.F.A., Goswami, P. and Zhou, T. (2013) Monsoons in a changing world: a regional perspective in a global context. *Journal of Geophysical Research: Atmospheres*, 118, 3053–3065. <https://doi.org/10.1002/JGRD.50258>.
- Koster, R.D., Dirmeyer, P.A., Guo, Z., Bonan, G., Chan, E., Cox, P., Gordon, C.T., Kanae, S., Kowalczyk, E., Lawrence, D., Liu, P., Lu, C.-H., Malyshev, S., McCavane, B., Mitchell, K., Mocko, D., Oki, T., Oleson, K., Pitman, A., Sud, Y.C., Taylor, C.M., Verseghy, D., Vasic, R., Xue, Y. and Yamada, T. (2004) Regions

- of strong coupling between soil moisture and precipitation. *Science*, 305, 1138–1140.
- Kubota, P. Y. (2012) *Variability of storage energy in the soil-canopy system and its impact on the definition of precipitation standard in South America*. PhD thesis, Instituto Nacional de Pesquisas Espaciais (INPE), São José dos Campos, Brazil (in Portuguese with abstract in English).
- Kumar, P. and Sarthi, P.P. (2021) Intraseasonal variability of Indian summer monsoon rainfall in CMIP6 models simulation. *Theoretical and Applied Climatology*, 145, 687–702.
- Liebmann, B. and Smith, C.A. (1996) Description of a complete (interpolated) outgoing longwave radiation dataset. *Bulletin of the American Meteorological Society*, 77, 1275–1277.
- Lu, R. and Dong, B. (2001) Westward extension of North Pacific subtropical high in summer. *Journal of the Meteorological Society of Japan*, 79, 1229–1241.
- Mitra, A. (2021) A comparative study on the skill of CMIP6 models to preserve daily spatial patterns of monsoon rainfall over India. *Frontiers Climate*, 3, 654763.
- Morrison, G., Curry, J.A. and Khvorostyanov, V.I. (2005) A new double moment microphysics parameterization for application in cloud and climate models. Part I: description. *Journal of the Atmospheric Sciences*, 62, 1665–1677. <https://doi.org/10.1175/JAS3446.1>.
- Morrison, H., Thompson, G. and Tatarskii, V. (2009) Impact of cloud microphysics on the development of trailing stratiform precipitation in a simulated squall line: comparison of one- and two-moment schemes. *Monthly Weather Review*, 137, 991–1007.
- Neale, R. and Slingo, J. (2003) The Maritime Continent and its role in the global climate: a GCM study. *Journal of Climate*, 16, 834–848. [https://doi.org/10.1175/1520-0442\(2003\)016<0834:TMCAIR>2.0.CO;2](https://doi.org/10.1175/1520-0442(2003)016<0834:TMCAIR>2.0.CO;2).
- Pascale, S., Bordoni, S., Kapnick, S.B., Vecchi, G.A., Jia, L., Delworth, T.L., Underwood, S. and Anderson, W. (2016) The impact of horizontal resolution on North American monsoon Gulf of California moisture surges in a suite of Coupled Global Climate Models. *Journal of Climate*, 29, 7911–7936.
- Raj, J., Bangalath, H.K. and Stenchikov, G. (2019) West African monsoon: current state and future projections in a high-resolution AGCM. *Climate Dynamics*, 52, 6441–6461. <https://doi.org/10.1007/s00382-018-4522-7>.
- Ridley, J., Menary, M., Kuhlbrodt, T., Andrews, M. and Andrews, T. (2018) *MOHC HadGEM3-GC31-LL model output prepared for CMIP6 CMIP*. United Kingdom: Earth System Grid Federation. <https://doi.org/10.22033/ESGF/CMIP6.419>.
- Rio, C. and Houdin, F. (2008) A thermal plume model for the convective boundary layer: representation of cumulus clouds. *Journal of the Atmospheric Sciences*, 65, 407–425.
- Robertson, A.W., Moron, V., Qian, J.-H., Chang, C.-P., Tangang, F., Aldrian, E., Koh, T.Y. and Juneng, L. (2011) The Maritime Continent monsoon. In: Chang, C.-P. (Ed.) *The Global Monsoon System: Research and Forecast*, 2nd edition. Singapore: World Scientific, pp. 85–98.
- Seneviratne, S.I., Corti, T., Davin, E.L., Hirschi, M., Jaeger, E.B., Lehner, I., Orlowsky, B. and Teuling, A.J. (2010) Investigating soil moisture–climate interactions in a changing climate: a review. *Earth-Science Reviews*, 99, 125–161.
- Slingo, A. (1989) A GCM parameterization for the shortwave properties of water clouds. *Journal of the Atmospheric Sciences*, 46, 1419–1427.
- Slingo, J.M. (1984) Cloud cover experimentation with the ECMWF model. In: *Workshop on Cloud Cover Parameterization in Numerical Models, 26–28 November 1984*. Reading: ECMWF, pp. 163–212.
- Slingo, J.M. (1987) The development of verification of a cloud prediction scheme for the ECMWF model. *Quarterly Journal of the Royal Meteorological Society*, 113, 899–927.
- Song, F. and Zhou, T. (2014a) The climatology and interannual variability of East Asian summer monsoon in CMIP5 coupled models: Does air–sea coupling improve the simulations? *Journal of Climate*, 27, 8761–8777.
- Song, F. and Zhou, T. (2014b) Interannual variability of East Asian summer monsoon simulated by CMIP3 and CMIP5 AGCMs: skill dependence on Indian Ocean–Western Pacific anticyclone teleconnection. *Journal of Climate*, 27, 1679–1697.
- Souza, D.C., Kubota, P.Y., Figueroa, S.N., Gutierrez, E.M.A.R. and Coelho, C.A.S. (2019) Impacto da resolução horizontal na simulação dos jatos de baixos níveis na América do Sul usando o modelo global do CPTEC. In: *Estudos Interdisciplinares nas Ciências Exatas e da Terra e Engenharias 4*, 82nd edition. Paraná, Brazil: Atena Editora, pp. 205–217.
- Tarasova, T. and Cavalcanti, I.F.A. (2002) Monthly mean solar radiative fluxes and cloud forcing over South America in the period of 1986–88: GCM results and satellite-derived data. *Journal of Applied Meteorology*, 41, 863–871. [https://doi.org/10.1175/1520-0450\(2002\)0412.0.CO;2](https://doi.org/10.1175/1520-0450(2002)0412.0.CO;2).
- Tarasova, T.A. and Fomin, B.A. (2000) Solar radiation absorption due to water vapor: advanced broadband parameterizations. *Journal of Applied Meteorology*, 39, 1947–1951.
- Tiedtke, M. (1989) A comprehensive mass flux scheme for cumulus parameterization in large-scale models. *Monthly Weather Review*, 117, 1779–1880.
- Toh, Y.Y., Turner, A.G., Johnson, S.J. and Holloway, C. (2018) Maritime Continent seasonal climate biases in AMIP experiments of the CMIP5 multimodel ensemble. *Climate Dynamics*, 50, 777–800. <https://doi.org/10.1007/s00382-017-3641-x>.
- Trenberth, K.E., Stepaniak, D.P. and Caron, J.M. (2000) The global monsoon as seen through the divergent atmospheric circulation. *Journal of Climate*, 13, 3969–3993.
- Veiga, S.F., Nobre, P., Giarolla, E., Capistrano, V., Baptista, M., Marquez, A.L., Figueroa, S.N., Bonatti, J.P., Kubota, P. and Nobre, C.A. (2019) The Brazilian Earth System Model ocean–atmosphere (BESM-OA) version 2.5: evaluation of its CMIP5 historical simulation. *Geoscientific Model Development*, 12, 1613–1642.
- Wang, B. and Ding, Q. (2008) Global monsoon: dominant mode of annual variation in the Tropics. *Dynamics of Atmospheres and Oceans*, 44, 165–183. <https://doi.org/10.1016/j.dynatmoce.2007.05.002>.
- Wang, B., and He, Q. (2019) Global monsoon summary. State of the Climate in 2019. *Special Supplement to the Bulletin of the American Meteorological Society*. 101, S200–S203.
- Wang, B., Jin, C. and Liu, J. (2020) Understanding future change of global monsoons projected by CMIP6 models. *Journal of Climate*, 33, 6471–6489. <https://doi.org/10.1175/JCLI-D-19-0993.1>.
- Wang, B., Kim, H.-K., Kikuchi, K. and Kitoh, A. (2011) Diagnostics metrics for evaluation of annual and diurnal cycles. *Climate Dynamics*, 37, 941–955. <https://doi.org/10.1007/s00382-010-0877-0>.

- Williams, K.D., Copsey, D., Blockley, E.W., Bodas-Salcedo, A., Calvert, D., Comer, R., Davis, P., Graham, T., Hewitt, H.T., Hill, R., Hyder, P., Ineson, S., Johns, T.C., Keen, A.B., Lee, R.W., Megann, A., Milton, S.F., Rae, J.G.L., Roberts, M.J., Scaife, A.A., Schiemann, R., Storkey, D., Thorpe, L., Watterson, I.G., Walters, D.N., West, A., Wood, R.A., Woollings, T. and Xavier, P. K. (2018) The Met Office Global Coupled Model 3.0 and 3.1 (GC3.0 and GC3.1) configurations. *Journal of Advances in Modeling Earth Systems*, 10, 357–380.
- Xin, X., Wu, T., Zhang, J., Yao, J. and Fang, Y. (2020) Comparison of CMIP6 and CMIP5 simulations of precipitation in China and the East Asian summer monsoon. *International Journal of Climatology*, 40, 6423–6440. <https://doi.org/10.1002/joc.6590>.
- Yang, M., Zhang, G.J. and Sun, D.Z. (2018) Precipitation and moisture in four leading CMIP5 models: biases across large-scale circulation regimes and their attribution to dynamic and thermodynamic factors. *Journal of Climate*, 31, 5089–5106.
- Yim, S.Y., Wang, B., Liu, J. and Wu, Z.W. (2014) A comparison of regional monsoon variability using monsoon indices. *Climate Dynamics*, 43, 1423–1437. <https://doi.org/10.1007/s00382-013-1956-9>.
- Yu, H., Kaufman, Y. J., Chin, M., Feingold, G., Remer, L. A., Anderson, T. L., Balkanski, Y., Bellouin, N., Boucher, O., Christopher, S., DeCola, P., Khan, R., Koch, D., Loeb, N., Reddy, M. S., Schultz, M., Takemura, T., and Zhou, M. (2006) A review of measurement-based assessments of the aerosol direct radiative effect and forcing. *Atmospheric Chemistry and Physics*, 6, 613–666.
- Zhang, W., Zhou, T. and Zou, L. (2019) Future intensification of the water cycle with an enhanced annual cycle over global land monsoon regions. *Journal of Climate*, 32, 5437–5452. <https://doi.org/10.1175/JCLI-D-18-0628.1>.
- Zhang, W., Zhou, T., Zou, L. and Chen, X. (2018a) Reduced exposure to extreme precipitation from 0.5C less warming in global land monsoon regions. *Nature Communications*, 9, 3153. <https://doi.org/10.1038/s41467-018-05633-3>.
- Zhang, L., Zhou, T., Klingaman, N.P., Wu, P. and Roberts, M. (2018b) Effect of horizontal resolution on the representation of the global monsoon annual cycle in AGCMs. *Advances in Atmospheric Sciences*, 35, 1003–1020. <https://doi.org/10.1007/s00376-018-7273-9>.
- Zhou, T., Turner, A.G., Kinter, J.L., Wang, B., Qian, Y., Chen, X., Wu, B., Wang, B., Liu, B., Zou, L. and He, B. (2016) GMMIP (v1.0) contribution to CMIP6: Global Monsoons Model Inter-comparison project. *Geoscientific Model Development*, 9, 3589–3604. <https://doi.org/10.5194/gmd-9-3589-2016>.
- Zhou, T., Yu, R., Li, H. and Wang, B. (2008) Ocean forcing to changes in global monsoon precipitation over the recent half-century. *Journal of Climate*, 21, 3833–3852.
- Zhou, T., Wu, B. and Wang, B. (2009a) How well do atmospheric general circulation models capture the leading modes of the interannual variability of the Asian-Australian monsoon? *Journal of Climate*, 22, 1159–1173.
- Zhou, T., Wu, B., Scaife, A.A., Brönnimann, S., Cherchi, A., Fereday, D., Fischer, A.M., Folland, C.K., Jin, K.E., Kinter, J.R., Knight, J.R., Kucharski, F., Kusunoki, S., Lau, N.-C., Li, L., Nath, M.J., Nakaegawa, T., Navarra, A., Pegion, P., Rozanov, E., Schubert, S., Sporyshev, P., Voldoire, A., Wen, X., Yoon, J.H. and Zeng, N. (2009b) The CLIVAR C20C project: Which components of the Asian-Australian monsoon circulation variations are forced and reproducible? *Climate Dynamics*, 33, 1051–1068.
- Zhou, T., Lu, J., Zhang, W. and Chen, Z. (2020a) The sources of uncertainty in the projection of global land monsoon precipitation. *Geophysical Research Letters*, 47, e2020GL088415. <https://doi.org/10.1029/2020GL088415>.
- Zhou, T., Zhang, W., Zhang, L., Zhang, X., Qian, Y., Peng, D., Ma, S. and Dong, B. (2020b) The dynamic and thermodynamic processes dominating the reduction of global land monsoon precipitation driven by anthropogenic aerosols emission. *Science China Earth Sciences*, 63, 919–933. <https://doi.org/10.1007/s11430-019-9613-9>.
- Zou, L., Zhou, T. and Peng, D. (2016) Dynamical downscaling of historical climate over CORDEX East Asia domain: a comparison of regional ocean atmosphere coupled model to standalone RCM simulations. *Journal of Geophysical Research: Atmospheres*, 121, 1442–1458. <https://doi.org/10.1002/2015JD023912>.

**How to cite this article:** Cavalcanti, I. F. A., Souza, D. C., Kubota, P. Y., Coelho, C. A. S., Figueroa, S. N., & Baker, J. C. A. (2022). The global monsoon system representation in BAM-v1.2 and HadGEM3 climate simulations. *International Journal of Climatology*, 42(15), 8089–8111. <https://doi.org/10.1002/joc.7694>